Received: 6 October 2023 | Revised: 22 February 2024 | Accepted: 7 March 2024

DOI: 10.1002/cne.25607

RESEARCH ARTICLE

JCN RESEARCH IN SYSTEMS NEUROSCIENCE THE JOURNAL OF COMPARATIVE NEUROLOGY WILEY

Anatomical organization of the cerebrum of the praying mantis *Hierodula membranacea*

Vanessa Althaus[1] | **Gesa Exner**[1,2] | **Joss von Hadeln**[1] | **Uwe Homberg**[1,2] | **Ronny Rosner**[1,3,4]

[1]Department of Biology, Animal Physiology, Philipps-University of Marburg, Marburg, Germany

[2]Center for Mind Brain and Behavior (CMBB), University of Marburg and Justus Liebig University of Giessen, Marburg, Germany

[3]Department of Biology, Institute of Developmental Biology and Neurobiology, Johannes Gutenberg University of Mainz, Mainz, Germany

[4]Biosciences Institute, Henry Wellcome Building for Neuroecology, Newcastle University, Framlington Place, Newcastle upon Tyne, UK

Correspondence
Ronny Rosner, Department of Biology, Institute of Developmental Biology and Neurobiology, Johannes Gutenberg University of Mainz, D-55128 Mainz, Germany. Email: rrosner@uni-mainz.de

Uwe Homberg, Department of Biology, Animal Physiology, Philipps-University of Marburg, D-35032 Marburg, Germany. Email: homberg@biologie.uni-marburg.de

Funding information
A Leverhulme Trust Reseach Leadership Award to Jenny Read supported RR and GE at Newcastle University, Grant/Award Number: RL-2012-019;
Deutsche Forschungsgemeinschaft, Grant/Award Number: HO 950/26-1

Abstract

Many predatory animals, such as the praying mantis, use vision for prey detection and capture. Mantises are known in particular for their capability to estimate distances to prey by stereoscopic vision. While the initial visual processing centers have been extensively documented, we lack knowledge on the architecture of central brain regions, pivotal for sensory motor transformation and higher brain functions. To close this gap, we provide a three-dimensional (3D) reconstruction of the central brain of the Asian mantis, *Hierodula membranacea*. The atlas facilitates in-depth analysis of neuron ramification regions and aides in elucidating potential neuronal pathways. We integrated seven 3D-reconstructed visual interneurons into the atlas. In total, 42 distinct neuropils of the cerebrum were reconstructed based on synapsin-immunolabeled whole-mount brains. Backfills from the antenna and maxillary palps, as well as immunolabeling of γ-aminobutyric acid (GABA) and tyrosine hydroxylase (TH), further substantiate the identification and boundaries of brain areas. The composition and internal organization of the neuropils were compared to the anatomical organization of the brain of the fruit fly (*Drosophila melanogaster*) and the two available brain atlases of Polyneoptera—the desert locust (*Schistocerca gregaria*) and the Madeira cock-

Abbreviations: ABR, anterior bridge; ACAR, accessory calyx ring; AL, antennal lobe; ALI, anterior lip; ALO, anterior lobe of the lobula complex; AMMC, antennal mechanosensory and motor center; AOT, anterior optic tract; AOTU, anterior optic tubercle; ATL, antler; AVLP, anterior ventrolateral protocerebrum; BU, bulb; CA, calyx; CB, central body; CBL, lower division of the CB; CBU, upper division of the CB; CL, clamp; CRE, crepine; CX, central complex; DAMMC, dorsal AMMC; EPA, epaulette; GA, gall; GABA, γ-aminobutyric acid; GC, great commissure; GLO, glomerular lobe; GOR, gorget; IB, inferior bridge; ICA, inner CA; ICL, inferior CL; IFS, inferior fiber system; INP, inferior neuropils; IT, isthmus tract; LAL, lateral accessory lobe; LALC, LAL commissure; LAMMC, lateral AMMC; LCA, lateral CA; LEF, lateral equatorial fascicle; LH, lateral horn; LLAL, lower LAL; LOX, lobula complex; LU, lower unit of the AOTU; LX, lateral complex; MAL, medial accessory lobe; mALT, medial antennal lobe tract; MAMMC, medial AMMC; MB, mushroom body; MBDL, median bundle; MCA, medial CA; ME, medulla; MEF, medial equatorial fascicle; ML, medial lobe; NO, noduli; OCA, outer CA; OCN, ocellar nerve; OLO, outer lobe of the LOX; OR, ocellar root; PB, protocerebral bridge; PED, pedunculus; PEDD, PED divide; PENP, periesophageal neuropils; PLP, posterior lateral protocerebrum; POC, posterior optic commissure; POTU, posterior optic tubercle; PS, posterior slope; PVLP, posterior ventrolateral protocerebrum; SCL, superior CL; SIP, superior intermediate protocerebrum; SLO, stalk lobe of the LOX; SLP, superior lateral protocerebrum; SMP, superior medial protocerebrum; SNP, superior neuropils; TC, tritocerebrum; TH, tyrosine hydroxylase; TUBUT, tubercle–bulb tract; ULAL, upper LAL; UU, upper unit of the AOTU; VES, vest; VFA, ventral area of flagellar afferents; VL, vertical lobe; VLNP, ventrolateral neuropils; VLP, ventrolateral protocerebrum; VMNP, ventromedial neuropils; VX, ventral complex; WED, wedge; WEDC, WED commissure.

roach (*Rhyparobia maderae*). This study paves the way for detailed analyses of neuronal circuitry and promotes cross-species brain comparisons. We discuss differences in brain organization between holometabolous and polyneopteran insects. Identification of ramification sites of the visual neurons integrated into the atlas supports previous claims about homologous structures in the optic lobes of flies and mantises.

KEYWORDS
3D reconstruction, brain atlas, *Hierodula membranacea*, insect brain, neuroanatomy, praying mantis

1 | INTRODUCTION

Insects show astonishing visual perception abilities employed for spatial orientation (Heinze et al., 2018; Merlin et al., 2012; Warrant & Dacke, 2011), object categorization (Avarguès-Weber et al., 2011; Giurfa, 2021), and object tracking (Gonzalez-Bellido et al., 2016; Nordström & O'Carroll, 2009; O'Carrol, 1993; Olberg, 2012), which often rival those of vertebrates. Understanding the neuroarchitectures that enable these abilities requires an in-depth analysis of brain areas and neuronal networks. The insect brain comprises neurons with cell bodies arranged in a peripheral cell body rind enclosing the neural processes and synaptic contacts in cell-body-free neuropils that are interconnected by axonal fiber tracts (Ito et al., 2014; Strausfeld, 1976). Certain brain areas like the central complex (CX) (Pfeiffer & Homberg, 2014), the antennal lobe (AL) (Schachtner et al., 2005), the optic lobe (Strausfeld, 2005), and the mushroom body (MB) (Fahrbach, 2006) are well-defined brain areas in the insect brain. These neuropils have been described in many insect species and are extensively studied, due to their pivotal roles in sensory–motor transformation, learning and memory (Kinoshita & Homberg, 2017; Strausfeld, 2012).

For a faithful comparison of morphological data from different specimens, standardized digital 3D brain atlases have been created by averaging the morphologies of 10 or more individual brains (el Jundi & Heinze, 2020; Rybak et al., 2010). Such atlases exist for the honeybee (Brandt et al., 2005), the fruit fly (Chiang et al., 2011), the desert locust (Kurylas et al., 2008), the Madeira cockroach (Wei et al., 2010), and the tobacco budworm (Kvello et al., 2009). These standard brains were largely designed to register the morphologies of individual neurons from different experiments into a common platform, but usually suffer from inclusion of only a small number of well-delineated brain areas such as the ALs, MBs, and CX. To overcome this problem, more detailed standard atlases were created for selected brain areas such as the CX and associated areas (el Jundi et al., 2010; Heinze et al., 2013; Kaiser et al., 2022). Many areas in the brain, however, are extensively interconnected and, thus, more difficult to identify and subdivide into distinct neuropils than the glia-ensheathed MBs or ALs. By clear definitions of boundaries, Ito et al. (2014) provided a detailed and comprehensive atlas of all brain areas in the fruit fly, which served as a template for comparative detailed subdivisions of the cerebrum across insects. Based on the criteria defined by Ito et al. (2014), fully segmented 3D digital brain atlases have been established for the ants *Cardiocondyla obscurior* (Bressan et al., 2015) and *Cataglyphis nodus* (Habenstein et al., 2020), the locust *Schistocerca gregaria* (von Hadeln et al., 2018), the monarch butterfly *Danaus plexippus* (Heinze & Reppert, 2012), the Bogong moth *Agrotis infusa* (Adden et al., 2020), the cockroach *Rhyparobia maderae* (Althaus et al., 2022), the honey bee *Apis mellifera* (Habenstein et al., 2023), and the dung beetles *Scarabaeus lamarcki* and *Scarabaeus satyrus* (Immonen et al., 2017). In contrast to the average standard brains, these detailed atlases are based on an individual immunolabeled brain that was reconstructed in detail.

This study provides a detailed 3D atlas of the brain of a third polyneopteran insect (Wipfler et al., 2019), the praying mantis (*Hierodula membranacea*). Being a predatory insect, it occupies an ecological niche that is different from that of the locust and cockroach. Behavioral studies in praying mantises examined prey recognition, distance perception, prey capture, mating behavior, and defensive behavior (Hurd, 1999; Kral & Prete, 1999; Nityananda, Bissianna, et al., 2016; Nityananda, Joubier, et al., 2019; Nityananda, O'Keeffe, et al., 2019; Poteser & Kral, 1995). Mantises are ambush predators that rely strongly on vision for hunting and spatial orientation. They are the only insect group known to use stereopsis for distance perception (Nityananda, Tarawneh, et al., 2016; Read, 2023; Rossel, 1983). Their compound eyes provide a nearly full panoramic view and exhibit binocular overlap in the frontal visual field (Rossel, 1979). Recent studies have examined the anatomical basis of visual performance in mantises in more detail. Their optic lobe comprises a larger volume than the central brain (Rosner et al., 2017) and consists of a thin lamina covering a large medulla (ME) and a joint lobula complex (LOX). The mantis LOX is highly segregated and consists of five neuropils. In contrast, the LOX of the closely related *R. maderae* shows a simpler organization into only three neuropils (Rosner et al., 2017). The composite structure of the LOX goes along with the processing of different aspects of the visual scenery. Intracellular recordings from individual neurons suggest that the processing of widefield motion is segregated from object motion (Rosner et al., 2019, 2020; Yamawaki, 2019).

To advance these functional insights on an anatomical level, we digitally segmented the cerebrum of the giant Asian mantis *H. membranacea*, one of the most commonly studied species, into distinct neuropils. While most neuropils have counterparts in the fruit fly, and the two other polyneopteran species studied, the desert locust

and Madeira cockroach, their relative volumes and shapes usually differ considerably. Integration of physiologically characterized visual interneurons into the 3D brain allows us now to clearly define their central targets. This will facilitate dissecting parallel visual inputs to the mantis brain with respect to prey recognition and capture as well as other visually driven behaviors.

2 | MATERIAL AND METHODS

2.1 | Animals

Praying mantises (*H. membranacea*) were obtained as nymphs from a commercial breeder (M&M Wüst). They were raised under a 12:12-h light/dark cycle and a temperature of 24°C at the Department of Biology of the University of Marburg. Animals used for single cell staining were kept as previously reported (Rosner et al., 2019, 2020) at 25°C at the Biosciences Institute of Newcastle University. The animals were fed with desert locusts or crickets. Only female mantises were used for the 3D atlas, for immunolabeling, and for the single-cell stainings that were used for integration into the atlas.

2.2 | Immunolabeling of whole mounts

Analysis of the different brain areas is largely based on whole mount brains labeled with antibodies against synapsin and supplemented by whole mount preparations immunolabeled for tyrosine hydroxylase (TH), the rate limiting enzyme in dopamine synthesis. Animals were cold-anesthetized for about 20 min at 4°C. Afterward, the head capsule of the animals was opened, and the brains were pre-fixed with 4% formaldehyde (FA) in phosphate-buffered saline (PBS; containing 78.8 mmol/L $Na_2HPO_4 \times 2H_2O$ and 19 mmol/L $NaH_2PO_4 \times H_2O$; pH 7.4) for 10–60 min. After prefixation, the brains were dissected (in PBS) and fixed overnight in 4% FA in PBS at 4°C. For TH immunolabeling, the brains were fixed overnight in 2% PFA in Millonig's phosphate buffer (containing 0.13 mol/L $NaH_2PO_4 \times H_2O$, 0.1 mol/L NaOH, 0.3 mmol/L $CaCl_2$, 1.2% glucose; pH 7.3–7.4). The next day, the brains were rinsed 4 × 10 min in 0.1 mol/L PBT (PBS, containing 5% Triton X-100, TrX). To facilitate penetration of the synapsin antibody, the brains were treated for 1 h with 1 mg/mL collagenase/dispase in 0.05 mol/L Tris-HCl (pH 7.6). After several washing steps, the brains were preincubated overnight with 5% normal goat serum (NGS; RRID: AB_2336990) in PBT (for TH immunostaining with extra 2% bovine serum albumin) at 4°C. Brains were incubated for 5 days at 4°C with anti-synapsin (mouse monoclonal, SYNORF1, 1:50, kindly provided by Drs. E. Buchner and C. Wegener, University of Würzburg; RRID: AB_2315425) or with the TH antibody (Immunostar, 1:1000; RRID: AB_572268) in a solution of 1% NGS in 0.1 mol/L PBT. After incubation, the brains were washed 3 × 10 min with PBT. For incubation with the secondary antibodies, the brains were transferred to cyanine-3-conjugated goat-anti-mouse (GaM-Cy3, 1:300, Jackson ImmunoResearch; RRID: AB_2338006) diluted in PBT with 1% NGS for 3 days at 4°C. The brains were finally rinsed 2 × 20 min in PBT and 3 × 20 min in PBS, followed by dehydration in an ascending ethanol series (25%, 50%, 70%, 90%, 95%, and 100%; 15 min each). For clearing the tissue, brains were transferred to a solution of 50% ethanol and 50% methyl salicylate (Merck) for 20 min and cleared for 20 min in 100% methyl salicylate. The whole mounts were embedded in Permount medium (Fisher Scientific) between two cover slips. Reinforcement rings were used as spacers.

2.3 | In vivo backfills of the antenna and maxillary palp

Animals were cold-anesthetized on ice for about 30 min. One maxillary palp or antenna was transected, and the cut nerve was submerged for 1 min in demineralized H_2O. The cut antennal nerve or maxillary nerve was subsequently placed in a drop of 4% Neurobiotin in 1 mol/L potassium chloride (KCl), sealed with petroleum jelly, and incubated at 4°C overnight in the refrigerator. The next day, the brains were dissected from the head capsule and transferred into fixative solution (4% paraformaldehyde [PFA], 0.25% glutaraldehyde, and 0.2% saturated picric acid; pH 7.4) in 0.1 mol/L PBS for 3 h at room temperature. Afterward, they were washed 3 × 15 min in 0.1 mol/L PBT (0.3% TrX). The brains were preincubated with 5% NGS in PBT for 1–2 h at room temperature and subsequently incubated with streptavidin-cyanine-3 (Strep-Cy3, 1:1,000, Dianova; RRID: AB_2337244) and anti-synapsin in a solution of 2% NGS in 0.1 mol/L PBT. After 3–4 days at 4°C, the brains were washed 4 × 10 min in PBT, followed by incubation in secondary antibody, goat-anti-mouse-cyanine-5 (GaM-Cy5, 1:300, Dianova), and Strep-Cy3 (1:1,000) in PBT with 2% NGS for 2–3 days at 4°C. Brains were, finally, washed 2 × 15 min in PBT and 2 × 15 min in PBS. Afterward, dehydration, clearing, and embedding of the whole mounts were performed as described above.

2.4 | Immunolabeling on 30-µm sections

To facilitate the establishment of neuropil boundaries, brain sections were labeled with antiserum against γ-aminobutyric acid (GABA) using the indirect peroxidase–antiperoxidase (PAP) technique (Sternberger, 1979). Brains of cold-anesthetized animals were dissected in 0.1 mol/L PBS from the head capsule. They were incubated in fixative containing 25% glutardialdehyde, 74% saturated picric acid, and 1% acetic acid for 4 h at room temperature. After rinsing 4 × 10 min in PBS and once in 0.1 mol/L PBT (0.3% TrX), the brains were frontally embedded in gelatin/albumin blocks and again fixed at 4°C in 8% PFA overnight for sectioning. The next day, the brains were sliced with a vibrating blade microtome (VT 1200 S; Leica Biosystems) in frontal plane to 30-µm sections, followed by preincubation for 1 h at room temperature in 8% NGS diluted in saline-substituted Tris buffer (SST; containing 1% TrX). Sections were incubated in anti-GABA antiserum raised in rabbit (1:8000, kindly provided by Dr. T. G. Kingan, University of Arizona; RRID: AB_2314457) in SST with 2% NGS for 20 h at room temperature. Following, brains were washed in SST (0.1% TrX) and transferred

to the secondary antibody solution, goat anti-rabbit IgG (1:40; RRID: AB_261363) in SST (containing 0.5% TrX and 1% NGS) for 1 h at room temperature. After rinsing in SST (0.1% TrX), sections were transferred to rabbit-PAP solution (1:300; RRID: AB_2315056) in SST (containing 0.5% TrX and 1% NGS) for 1 h. To remove excess PAP, the brains were washed 5 × 10 min with SST (0.5% TrX). 3,3′-Diaminobenzidine tetrahydrochloride (DAB; 0.03 mg/mL) was applied to the sections with H_2O_2 (0.02%) in 0.1 mol/L phosphate buffer (pH 7.4). After staining, the sections were washed for 3 × 10 min in phosphate buffer to stop the reaction and mounted on coated microscope slides. Afterward, the sections were dehydrated in an ascending ethanol series, cleared in xylenes, and mounted in Entellan (Merck) under cover slips.

2.5 | Antibody characterization

The anti-GABA antiserum (# 9/24, provided by T. G. Kingan; RRID: AB_2314457) is an affinity-purified antiserum raised in rabbit against conjugates of GABA–glutaraldehyde–keyhole limpet hemocyanin (KLH; Hoskins et al., 1986). The antiserum has been used to characterize GABA-immunoreactive neurons in many insect species, including the praying mantis *H. membranacea* (Homberg et al., 2018; Rosner et al., 2017). On brain sections of the sphinx moth *Manduca sexta*, immunostaining was abolished by preadsorption of the diluted antiserum with 24 nmol/L GABA–KLH conjugates, but staining was not reduced by preadsorption with conjugates of L-glutamic acid, L-glutamine, taurine, or β-alanine (Hoskins et al., 1986). Preadsorption of the diluted antiserum with 50 µmol/L GABA–glutaraldehyde complex abolished all immunostaining on vibratome sections of *H. membranacea* brains (Rosner et al., 2017).

The monoclonal antibody against synapsin (#3C11, SYNORF1; RRID: AB_2315425) was obtained from Drs. E. Buchner and C. Wegener. It was raised in mice against fusion proteins consisting of glutathione-S-transferase and parts of the *Drosophila melanogaster* synaptic vesicle protein SYN1 (Klagges et al., 1996). Its specificity has been demonstrated in *D. melanogaster* by Klagges et al. (1996). The antibody labels synaptic neuropils as shown in different insect species, including *H. membranacea* (Rosner et al., 2017).

The monoclonal TH antibody (Immunostar, cat# 22941; RRID: AB_572268) was raised in mouse against full-length TH purified from rat PC12 cells. The antibody recognizes an epitope in the catalytic core of the TH, which is highly conserved during evolution (Calvo et al., 2011). Being the rate-limiting enzyme in dopamine synthesis, the antibody labels putatively dopaminergic neurons in a wide range of animals including various insect species (Hamanaka et al., 2016; Timm et al., 2021). Staining patterns obtained with the TH antibody and a dopamine antiserum were highly similar in the brain of a cockroach (Hamanaka et al., 2016) and a locust (Timm et al., 2021). In immunoblots of brain homogenates from crickets, backswimmer, cockroaches, and water strider, the antibody labels a single lane at 54–66 kDa (Hamanaka et al., 2016; Timm et al., 2021), which corresponds well with the molecular weight of human TH (60 kDa; Immunostar).

2.6 | Image acquisition

Fluorescently labeled whole-mount preparations and sections were scanned by a confocal laser scanning microscope (Leica, TCS SP5; Leica Microsystems). Preparations were scanned with a 20× oil immersion objective lens (HC PL APO 20×/0.75 Imm Corr CS2). Cy3 fluorescence was excited by a diode-pumped solid-state laser (561 nm, DPSS 10 mW) and the Cy5 fluorescence with a helium neon laser (633 nm, HeNe 10 mW). The synapsin-stained whole mounts were scanned at a resolution of 1024 × 1024 pixels in the *xy*-plane (pixel size: 0.75 × 0.75 µm), with a *z*-step size of 1 µm, a line average of 4, and scanning velocity of 400 Hz for the synapsin labeling and a line average of 2 for the backfills. The resulting data stacks were further processed in Amira 6.5 and 5.6 (Thermo Fisher Scientific).

Images of GABA-labeled sections were obtained using a digital camera (ProgRes C12plus; Jenoptik) connected to a transmission light microscope (Axioskop; Zeiss). Contrast and brightness of the images were adjusted in Affinity Photo (Serif), and the final figures of all created images were made in Affinity Designer (Serif).

2.7 | Anatomical reconstruction of neuropils and neurons

Three-dimensional reconstructions of neuropils were created with the software Amira 6.5. Sequential scans of a selected synapsin-labeled whole-mount brain were opened and processed in the *Segmentation editor*. Boundaries of the neuropils were set manually by comparing synapsin labeling with GABA and TH immunostaining. Levels of neuropils, in which boundaries to neighboring structures like fiber tracts were particularly obvious, were marked in all planes of the image stack resulting in a 3D grid that built the basis for a polygonal surface. To generate a 3D model from the grid, we used the *Wrap*-module. It created a polygonal surface, which was visualized using *SurfaceGen* and displayed with *SurfaceView*. To smooth and minimalize the generated data size, the reconstruction was *Simplified*. We reconstructed neuropils and, in addition, some fiber tracts and commissures that were used as boundaries between these neuropils. The number of glomeruli in the AL was counted using the *Landmark* tool.

We identified the arborization areas of seven visual interneurons that were recorded and labeled by Neurobiotin injections in previous studies (Rosner et al., 2019, 2020). Four of these neurons were published in Rosner et al. (2020) and the other three in Rosner et al. (2019). The reconstruction of the individual neurons was done in Amira 5.6 by using the *Skeletonize* plugin. Neurites, somata, and branches were manually traced in the confocal data stacks by fitting the diameter and path of each part/segment of the neuron corresponding to the gray values in the staining. The complete reconstructions of all seven neurons were integrated into the 3D atlas to identify their arborization areas in the cerebrum in detail, in addition to their innervation sites in the optic lobes examined previously (Rosner et al., 2019, 2020).

2.8 | Integration of neurons in the mantis brain atlas

Neuron integration was performed manually using Amira 6.5. For each neuron, three associated neuropils of the cerebrum were individually 3D-reconstructed within the brain containing the stained neuron to ensure a correct spatial arrangement. The integration process began by transforming the individually reconstructed neuropils into the corresponding neuropils of the brain atlas. Alignments were based on adjustments in translation, rotation, and isotropic scaling, using the *Transform editor*. Once both reconstructions were aligned with the atlas, the transformation parameters from the three reconstructed neuropils were transferred to the associated neuron using the console commands > *getTransform*, > *setTransform*, and > *applyTransform*. Accurate integration of the neurons was confirmed by closely matching neuron positions in the brain of origin and the 3D brain atlas.

3 | RESULTS

We reconstructed 42 major neuropils, some with additional subunits, and 12 fiber tracts and commissures of the cerebrum from a mature female mantis *H. membranacea* (Figure 1; Video S1). The reconstruction is based on a synapsin-immunolabeled whole-mount brain and additional data from GABA-immunolabeled brain sections, TH immunolabeling, individually injected neurons, and backfills of the antennal flagellum and maxillary palp. To facilitate the identification of neuropils and fiber tracts, a series of annotated frontal optical sections through the mantis brain is provided in Figures 2–5. Neuropil boundaries were set based on the criteria of Ito et al. (2014). For the periesophageal neuropils (PENP), the 3D reconstructions of the locust (von Hadeln et al., 2018) and the cockroach (Althaus et al., 2022) brains were used as references, because correspondence of these brain areas in polyneopteran insects with those in the fly and other Holometabola has not yet been resolved. The optic lobe is not included here, because a 3D reconstruction of optic-lobe neuropils was already provided by Rosner et al. (2017). This study will facilitate neural network analyses in the mantis brain. To demonstrate these possibilities, we integrated seven neurons previously characterized by Rosner et al. (2019, 2020) into the 3D-reconstructed brain.

3.1 | Mushroom body

The MBs are distinct bilaterally paired neuropils in the cerebrum of *H. membranacea*. Each MB comprises a pedunculus (PED), a medial lobe (ML), a vertical lobe (VL), two calyces (CAs), each consisting of an inner (ICA) and outer calyx (OCA), and an accessory calyx ring (ACAR). The MBs extend from the level of the central body (CB) to the dorsal surface and through the whole depth of the protocerebrum (Figure 6a,b).

In each brain hemisphere, two cup-shaped structures—a medial (MCA) and a lateral CA (LCA)—are present. The cups in each hemisphere are fused (Figures 4b,c, 5 and 6a–c) and are the most dorsal neuropils in the mantis cerebrum. Each cup is further subdivided into an inner (ICA) and outer (OCA) structure. The ICAs consist of fiber bundles of Kenyon cells (Strausfeld & Li, 1999) and can be seen as extensions of the PED (Figure 6e). They are free of GABA immunolabeling (Figure 6e) and show only weak synapsin staining (Figure 6c). In contrast, the OCAs are densely innervated by GABA-immunolabeled neurons and thereby clearly distinguishable from the rest of the MB (Figure 6e). A ring-shaped neuropil, the ACAR, emerges ventrally attached to the CAs and spans around both strands of the PED (Figures 4c, 5a, and 6a,b). It shows a smooth texture of synapsin immunolabeling, but conspicuous accumulations of synapsin (Figure 6d), which is unique to the region of the ACAR.

The point of fusion of the ML, VL, and PED, called PED divide (PEDD; Figure 6b), is located at the anterior-most part of the MB. The PEDD was not reconstructed as an individual neuropil, because it could not be distinguished from the lobes by synapsin immunolabeling (Figure 2b,c). Furthermore, no structural equivalent of a spur, a small lateral protrusion of the PEDD described in *S. gregaria* (von Hadeln et al., 2018), *A. infusa* (Adden et al., 2020), and *D. melanogaster* (Ito et al., 2014; Tanaka et al., 2008), but not in *R. maderae* (Althaus et al., 2022), was found. The ML extends horizontally from the PEDD toward the brain midline, nearly touching its contralateral counterpart, but without apparent fusion (Figures 2b,c, 3 and 4a,b). Adjacent to the ML, the medial accessory lobe (MAL) is positioned ventrally, while the anterior lip (ALI) and CB are dorsally to the ML (Figures 3 and 4a,b). The VL extends dorsally from the PEDD, passing through the protocerebrum. Its dorsal tip almost contacts the ventral border of the MCA. Both the VL and PED are essential landmarks for defining boundaries of the superior (SNP) and inferior neuropils (INP). The VL touches laterally the superior clamp (SCL) and medially the ALI, a small bulge of the crepine (CRE), and the superior medial protocerebrum (SMP). It shows, similar to the ML, smoothly structured synapsin labeling and was easily identified by its concise borders (Figures 2b,c, 3 and 4a,b). The PED leaves the PEDD laterally and is ventrolaterally limited by the extension of the anterior (AVLP) and posterior ventrolateral protocerebrum (PVLP). The PED extends through the inferior protocerebrum and turns dorsally between the superior lateral protocerebrum (SLP) and inferior clamp (ICL) toward the CAs (Figures 2b,c, 3, 4, and 5a,b). Near its dorsal end, the PED bifurcates at the region of the PED neck. The PED neck was not reconstructed as a separate neuropil, because it was not recognizable by synapsin immunolabeling. However, it is located at the point of fusion of the two strands of Kenyon cell axons originating from the MCA and LCA (Figure 6e).

3.2 | CX, ALI, and lateral complex

The CX is a midline crossing group of neuropils (Figure 6h) and comprises the CB, the protocerebral bridge (PB), and the paired noduli (NO). The CB is composed of an upper (CBU) and a lower division (CBL), both having a semitoroidal shape. The CBU is larger than the CBL and encases the latter dorsoposteriorly (Figures 4 and 6i–g). In *D. melanogaster*, the equivalents are referred to as the fan-shaped

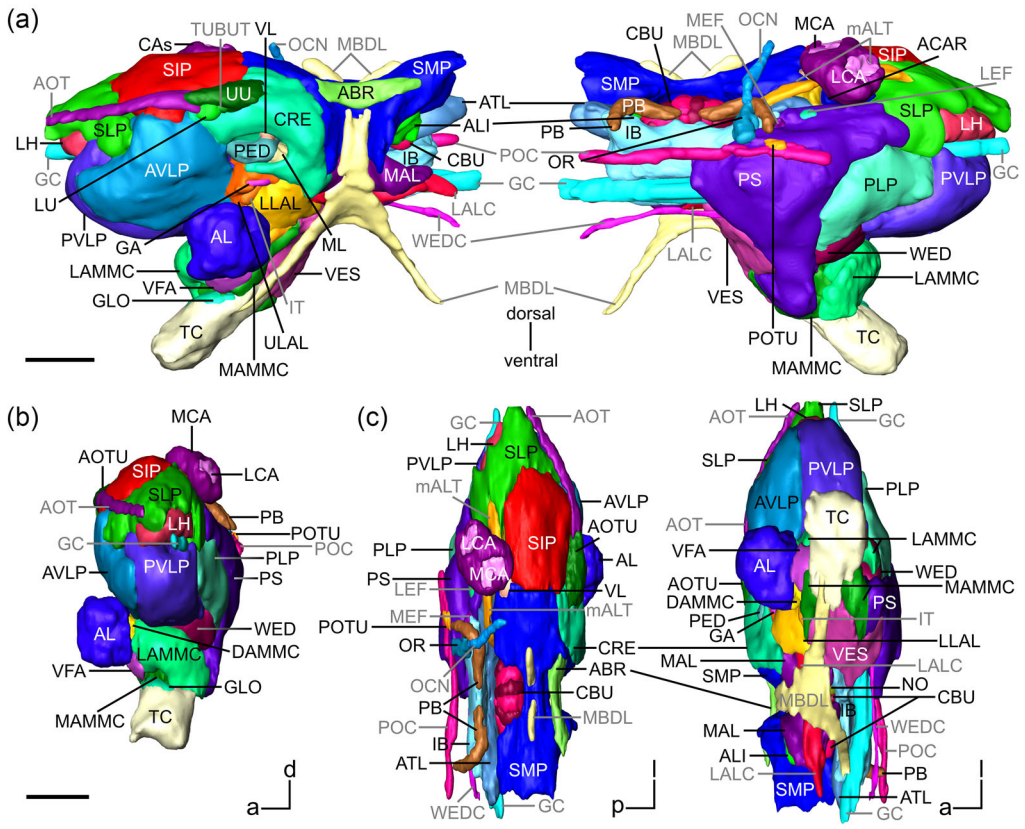

FIGURE 1 Three-dimensional reconstruction of the cerebrum of the mantis. (a) Anterior (left) and posterior (right), (b) lateral, and (c) dorsal (left) and ventral (right) views of the reconstructed neuropils (labeled in black) and tracts, fiber systems, and commissures (labeled in gray) of the mantis brain. a, anterior; ABR, anterior bridge; ACAR, accessory calyx ring; AL, antennal lobe; ALI, anterior lip; AMMC, antennal mechanosensory and motor center; AOT, anterior optic tract; AOTU, anterior optic tubercle; ATL, antler; AVLP, anterior ventrolateral protocerebrum; CA, calyx; CBU, upper division of the central body; CRE, crepine; d, dorsal; DAMMC, dorsal AMMC; GA, gall; GC, great commissure; GLO, glomerular lobe; IB, inferior bridge; IT, isthmus tract; l, lateral; LAL, lateral accessory lobe; LALC, LAL commissure; LAMMC, lateral AMMC; LCA, lateral CA; LEF, lateral equatorial fascicle; LH, lateral horn; LLAL, lower LAL; LU, lower unit of the AOTU; MAL, medial accessory lobe; mALT, medial antennal lobe tract; MAMMC, medial AMMC; MBDL, median bundle; MCA, medial CA; MEF, medial equatorial fascicle; ML, medial lobe; NO, noduli; OCN, ocellar nerve; OR, ocellar root; p, posterior; PB, protocerebral bridge; PED, pedunculus; PLP, posterior lateral protocerebrum; POC, posterior optic commissure; POTU, posterior optic tubercle; PS, posterior slope; PVLP, posterior ventrolateral protocerebrum; SIP, superior intermediate protocerebrum; SLP, superior lateral protocerebrum; SMP, superior medial protocerebrum; TC, tritocerebrum; ULAL, upper LAL; UU, upper unit of the AOTU; v, ventral; VES, vest; VFA, ventral area of flagellar afferents; VL, vertical lobe; WED, wedge; WEDC, WED commissure. Scale bars = 200 μm.

body (FB) and ellipsoid body (EB), respectively, denoting their distinct shapes. Both subdivisions of the CB are surrounded by a large mass of fibers. They are covered by the SMP and the ALI (anterior), and the inferior bridge (IB) and the antler (ATL; posterior). We distinguished 10 vertical slices in the CBU based on synapsin immunolabeling and GABA immunolabeling, consistent with the findings of Rosner et al. (2017). Although we could not discern horizontal layers of the CBU, Timm et al. (2021) identified at least three layers using TH immunolabeling. Similar to the CBU, the CBL is composed of 10 bean-like vertical subunits, five per hemisphere. As reported by Rosner et al. (2017), the outermost columns (R5, L5) in the CBL and CBU are noticeably smaller than the other slices. GABA-immunolabeled fibers of tangential neurons enter the CBL through the isthmus tract (IT) and give rise to strong immunostaining in the columns of the CBL (Figure 6g).

The paired NO (Figures 4b,c and 6h) are located ventral to the CB. They are small neuropils, in most insect species separated into upper and lower units, but we were unable to identify these subunits here. The third neuropil of the CX is the paired PB (Figures 5b,c and 6j). Positioned dorsoposterior to the CB, the PB consists of two elongated neuropils that bend laterally in posterior direction, resembling a handlebar shape as a whole. The two arms, one in each brain hemisphere, are spatially separated but connected by a fiber bundle crossing the midline.

The ALI is a slender elongated synapsin-rich area (Figure 3) that extends horizontally across the brain midline, directly anterior to the CB. The ALI appears anteriorly between the CREs, VLs, and MLs of both hemispheres (Figure 3). The SMP and the CRE are the dorsal and anterior limits of the ALI, respectively. A small region ventrolateral to the ALI was assigned to the CRE based on GABA immunolabeling. While

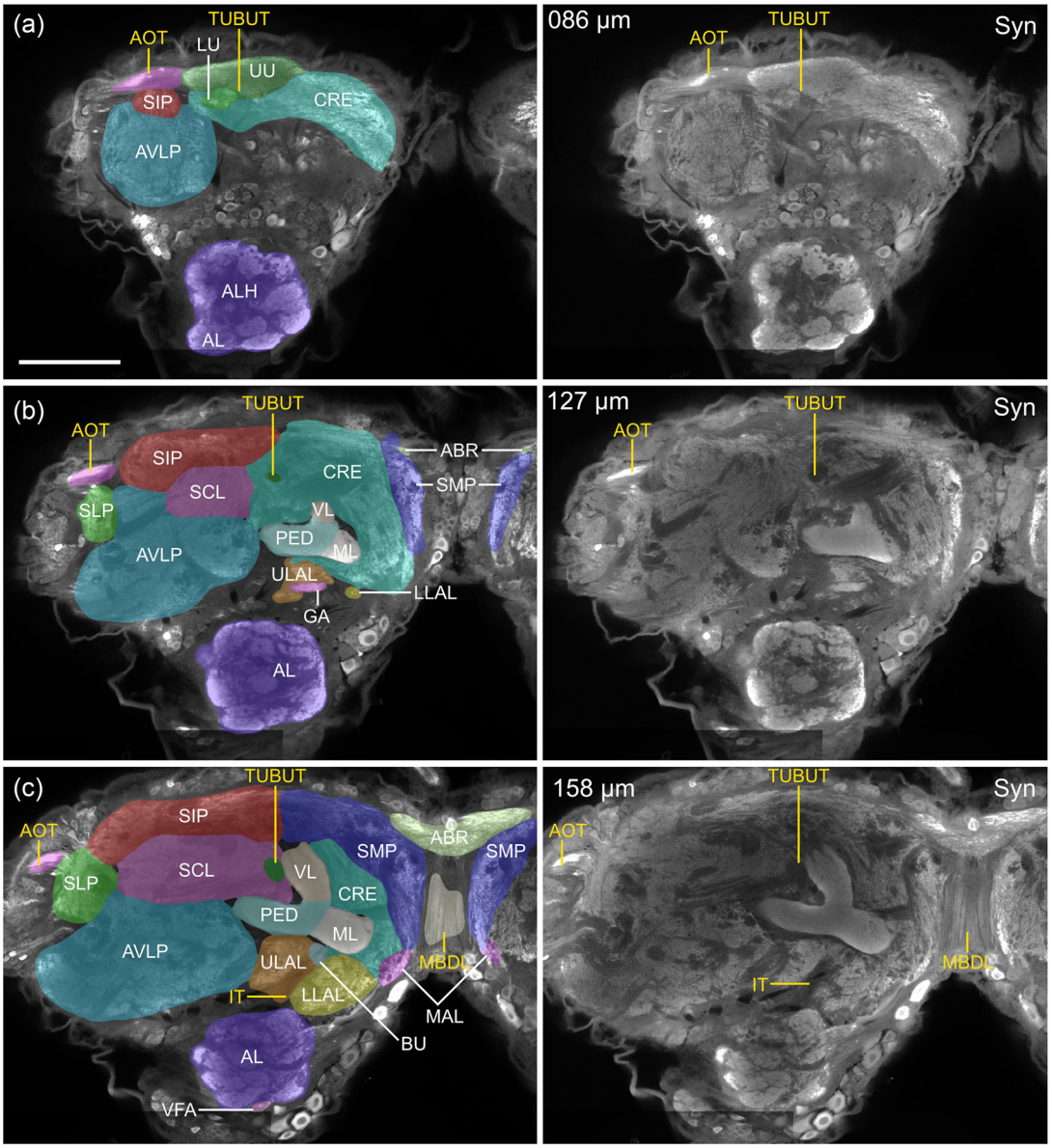

FIGURE 2 Series of frontal optical sections through the mantis brain from a depth of 86 µm relative to the anterior brain surface (a) to a depth of 158 µm (c). Right panels show synapsin immunolabeling in confocal sections, and left panels show the same sections overlayed with a transparent surface cut of the three-dimensional reconstructions. Tracts, fiber systems, and commissures are labeled in yellow and neuropils in white. ABR, anterior bridge; AL, antennal lobe; ALH, AL hub; AOT, anterior optic tract; AOTU, anterior optic tubercle; AVLP, anterior ventrolateral protocerebrum; BU, bulb; CRE, crepine; GA, gall; IT, isthmus tract; LAL, lateral accessory lobe; LLAL, lower LAL; LU, lower unit of the AOTU; MAL, medial accessory lobe; MBDL, median bundle; ML, medial lobe; PED, pedunculus; SCL, superior clamp; SIP, superior intermediate protocerebrum; SLP, superior lateral protocerebrum; SMP, superior medial protocerebrum; Syn, synapsin; TUBUT, tubercle–bulb tract; ULAL, upper LAL; UU, upper unit of the AOTU; VFA, ventral area of flagellar afferents; VL, vertical lobe. Scale bar = 200 µm.

the CRE is widely pervaded by GABA-immunolabeled fibers, the ALI is nearly devoid of GABA staining (Figure 6f). In holometabolous insects such as the fruit fly *D. melanogaster*, the ALI has not been observed as a distinct neuropil, but in other Polyneoptera like the cockroach *R. maderae* or locust *S. gregaria*, the ALI is closely associated with the CX (Jahn et al., 2023; Timm et al., 2021; von Hadeln et al., 2020).

Another prominent CX-associated neuropil group is the lateral complex (LX; Figure 7). It is divided into the bulb (BU) and the lateral accessory lobe (LAL), which is further subdivided into the lower (LLAL) and upper (ULAL) LAL, along with the gall (GA). The LAL is positioned ventrolaterally from the CX and is, among other criteria, characterized by the quite prominent LAL commissure (LALC) that connects the bilateral LALs across the brain midline segregating the LLAL from the ULAL (Figure 3b,c). The LAL is further traversed by the IT, a major fiber bundle containing GABA-labeled neurites that connect the LX and CX. The IT courses from the CX through the LAL and serves as an additional boundary between the ULAL, LLAL, and BU (Figure 7a,b,c'). The ULAL (Figures 2b,c, 3, and 4a) emerges at the anterior surface of the

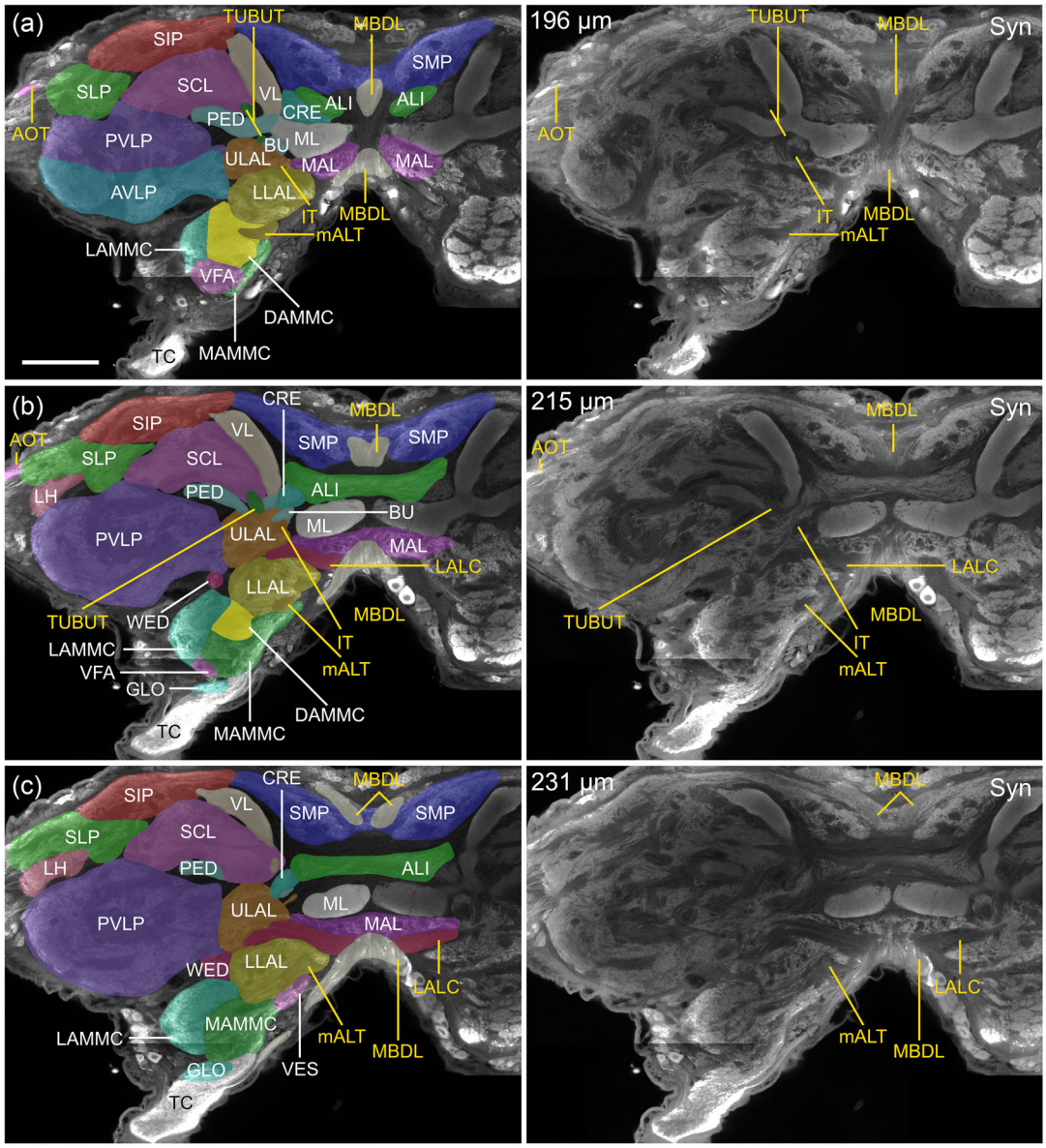

FIGURE 3 Series of frontal optical sections through the mantis brain from a depth of 196 µm (a) to a depth of 231 µm (c). Right panels show confocal sections of synapsin immunolabeling, and left panels show the same sections overlayed with a transparent surface cut of the three-dimensional reconstructions. Tracts, fiber systems, and commissures are labeled in yellow and neuropils in white. ALI, anterior lip; AMMC, antennal mechanosensory and motor center; AOT, anterior optic tract; AVLP, anterior ventrolateral protocerebrum; BU, bulb; CRE, crepine; DAMMC, dorsal AMMC; GLO, glomerular lobe; IT, isthmus tract; LAL, lateral accessory lobe; LALC, LAL commissure; LAMMC, lateral AMMC; LH, lateral horn; LLAL, lower LAL; LU, lower unit of the AOTU; MAL, medial accessory lobe; mALT, medial antennal lobe tract; MAMMC, medial AMMC; MBDL, median bundle; ML, medial lobe; PED, pedunculus; PVLP, posterior ventrolateral protocerebrum; SCL, superior clamp; SIP, superior intermediate protocerebrum; SLP, superior lateral protocerebrum; SMP, superior medial protocerebrum; Syn, synapsin; TC, tritocerebrum; TUBUT, tubercle–bulb tract; ULAL, upper LAL; VES, vest; VFA, ventral area of flagellar afferents; VL, vertical lobe; WED, wedge. Scale bar = 200 µm.

cerebrum between the PED, ML, and AL. It is, thus, posteriorly and medioventrally attached by the LLAL, separated by the LALC and the IT. The VL adjoins at the dorsal surface of the ULAL, the ventrolateral protocerebrum (VLP) laterally, and the MAL and LLAL medially. The posterior boundaries are demarcated by the appearance of the epaulette (EPA) and the great commissure (GC), which is noticeably large in the mantis. The medial antennal lobe tract (mALT) serves as a landmark indicating the posterior boundary of the LAL (Figure 4a,b), as described in the locust (von Hadeln et al., 2018) and the cockroach (Althaus et al., 2022), together with the inferior fiber system (IFS). Its medial boundaries (Figures 2b,c, 3 and 4a) from anterior to posterior include the cell body rind, median bundle (MBDL), mALT, vest (VES), and MAL. Ventrally, the LAL is delimited by the mALT, IFS, and the neuropils of the antennal mechanosensory and motor center (AMMC).

The uniform BU is embedded dorsoanteriorly between the ULAL and LLAL. It lies posterior to the CRE, anterolateral to the IT, and

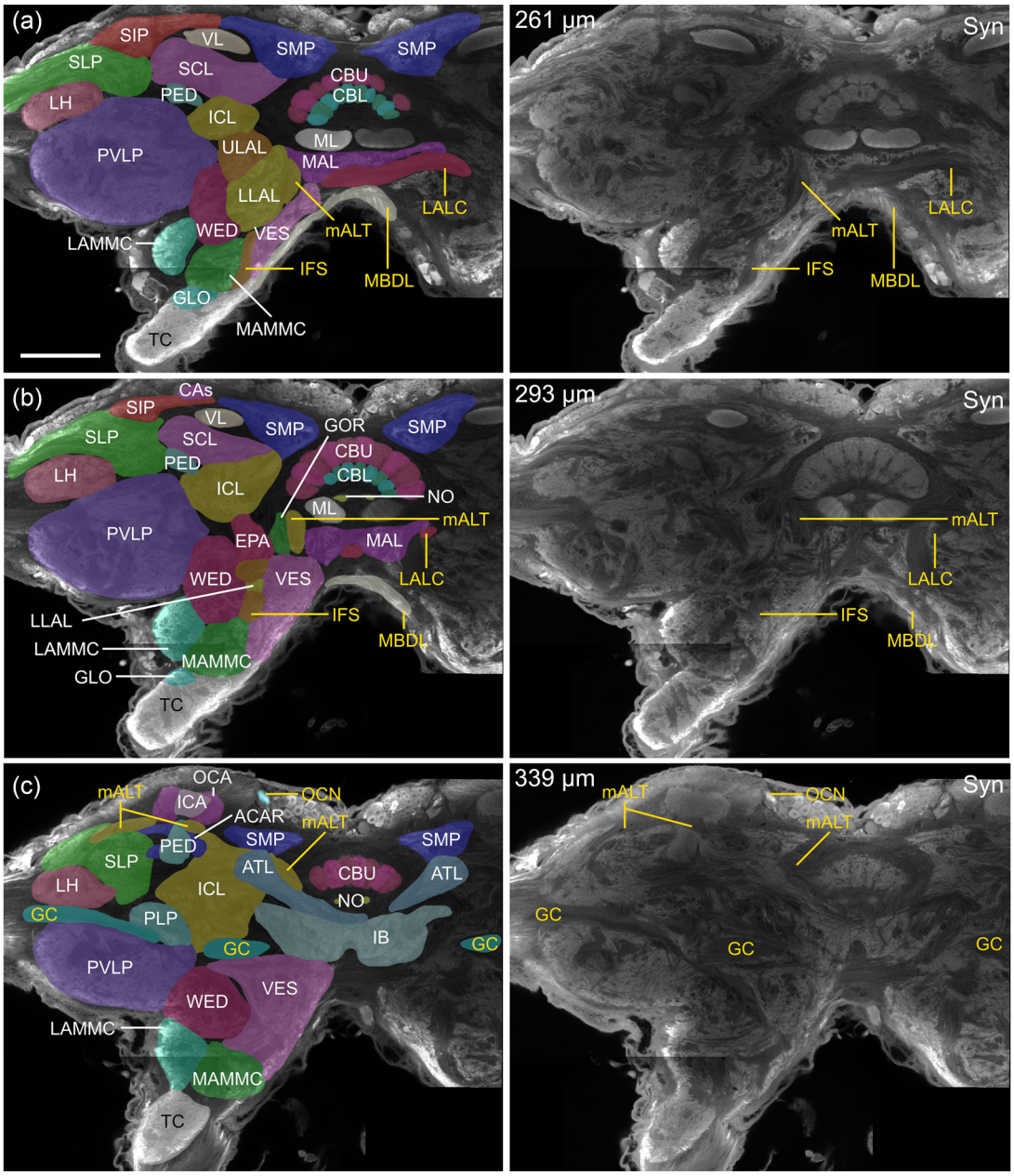

FIGURE 4 Series of frontal optical sections through the mantis brain from a depth of 261 µm (a) to a depth of 339 µm (c). Right panels show confocal sections of synapsin immunolabeling, and left panels show the same sections overlayed with a transparent surface cut of the three-dimensional reconstructions. Tracts, fiber systems, and commissures are labeled in yellow and neuropils in white. ACAR, accessory CA ring; AMMC, antennal mechanosensory and motor center; ATL, antler; CA, calyx; CB, central body; CBL, lower division of the CB; CBU, upper division of the CB; EPA, epaulette; GC, great commissure; GLO, glomerular lobe; GOR, gorget; IB, inferior bridge; ICA, inner CA; ICL, inferior clamp; IFS, inferior fiber system; LAL, lateral accessory lobe; LALC, LAL commissure; LAMMC, lateral AMMC; LH, lateral horn; LLAL, lower LAL; MAL, medial accessory lobe; mALT, medial antennal lobe tract; MAMMC, medial AMMC; MBDL, median bundle; ML, medial lobe; NO, noduli; OCA, outer CA; OCN, ocellar nerve; PED, pedunculus; PLP, posterior lateral protocerebrum; PVLP, posterior ventrolateral protocerebrum; SCL, superior clamp; SIP, superior intermediate protocerebrum; SLP, superior lateral protocerebrum; SMP, superior medial protocerebrum; Syn, synapsin; TC, tritocerebrum; ULAL, upper LAL; VES, vest; VL, vertical lobe; WED, wedge. Scale bar = 200 µm.

ventral to the PED/ML (Figures 2c, 3a,b, 6f, and 7c'). The BU was identified by its finer and denser synapsin staining compared to surrounding regions, as well as intense GABA immunolabeling (Figure 6f), as it houses the dendrites of GABA-immunoreactive tangential neurons of the CBL. Furthermore, we discovered the tubercle–bulb tract (TUBUT), which connects the anterior optic tubercle (AOTU) with the BU (Figures 2 and 3a,b).

The GA, characterized as a distinct area of axonal projections of CX outputs in *D. melanogaster* (Wolff et al., 2015), the dung beetles *S. lamarcki* and *S. satyrus* (el Jundi et al., 2018), the cockroach *R. maderae*

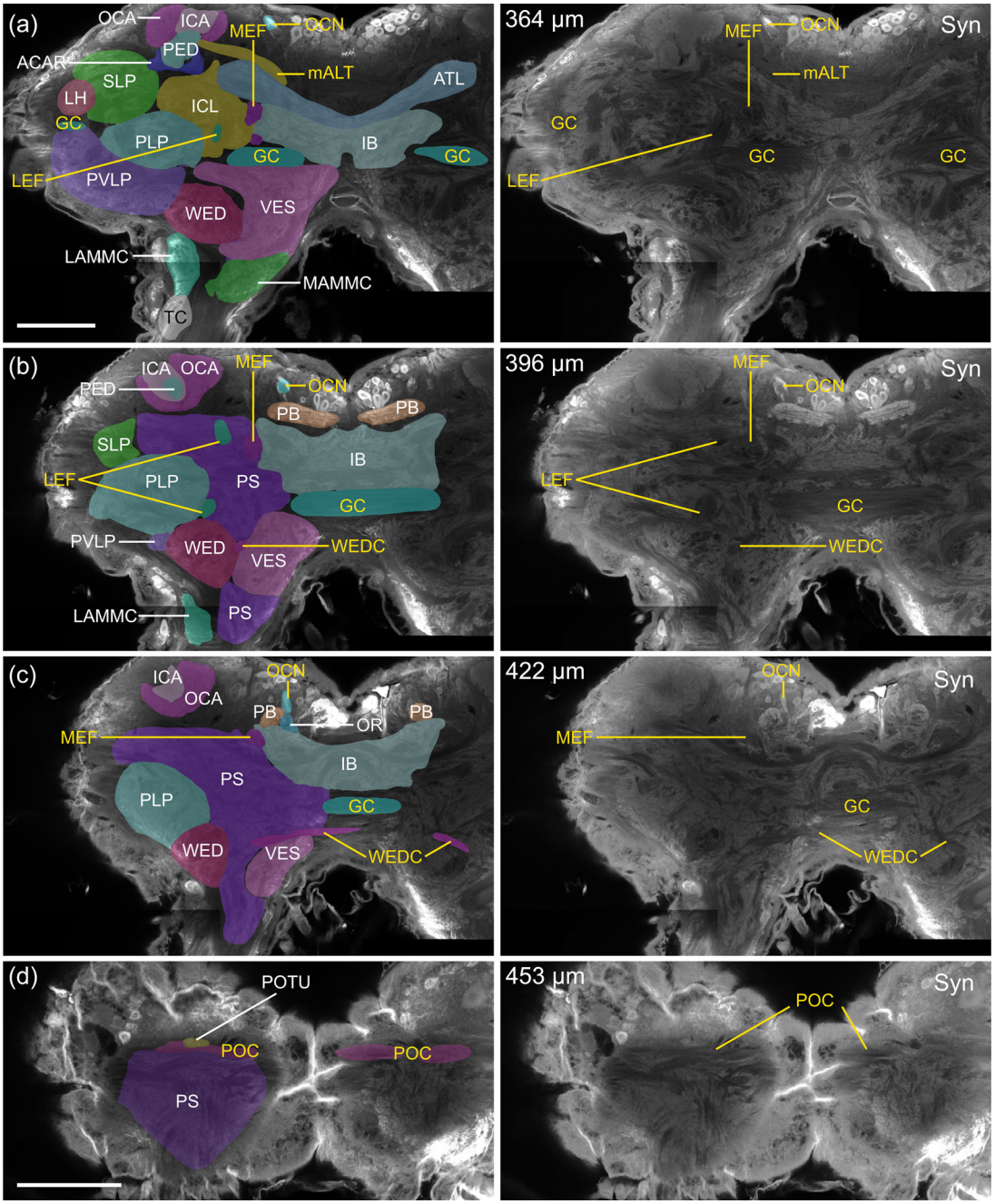

FIGURE 5 Series of frontal optical sections through the mantis brain from a depth of 364 µm (a) to a depth of 453 µm (d). Right panels show confocal sections of synapsin immunolabeling, and left panels show the same sections overlayed with a transparent surface cut of the three-dimensional reconstructions. Tracts, fiber systems, and commissures are labeled in yellow and neuropils in white. ACAR, accessory CA ring; AMMC, antennal mechanosensory and motor center; ATL, antler; CA, calyx; GC, great commissure; IB, inferior bridge; ICA, inner CA; ICL, inferior clamp; LAMMC, lateral AMMC; LEF, lateral equatorial fascicle; LH, lateral horn; mALT, medial antennal lobe tract; MAMMC, medial AMMC; MEF, medial equatorial fascicle; OCA, outer CA; OCN, ocellar nerve; OR, ocellar root; PB, protocerebral bridge; PED, pedunculus; PLP, posterior lateral protocerebrum; POC, posterior optic commissure; POTU, posterior optic tubercle; PS, posterior slope; PVLP, posterior ventrolateral protocerebrum; SLP, superior lateral protocerebrum; Syn, synapsin; TC, tritocerebrum; VES, vest; WED, wedge; WEDC, WED commissure. Scale bars = 200 µm (a, applies to b and c), 200 µm (d).

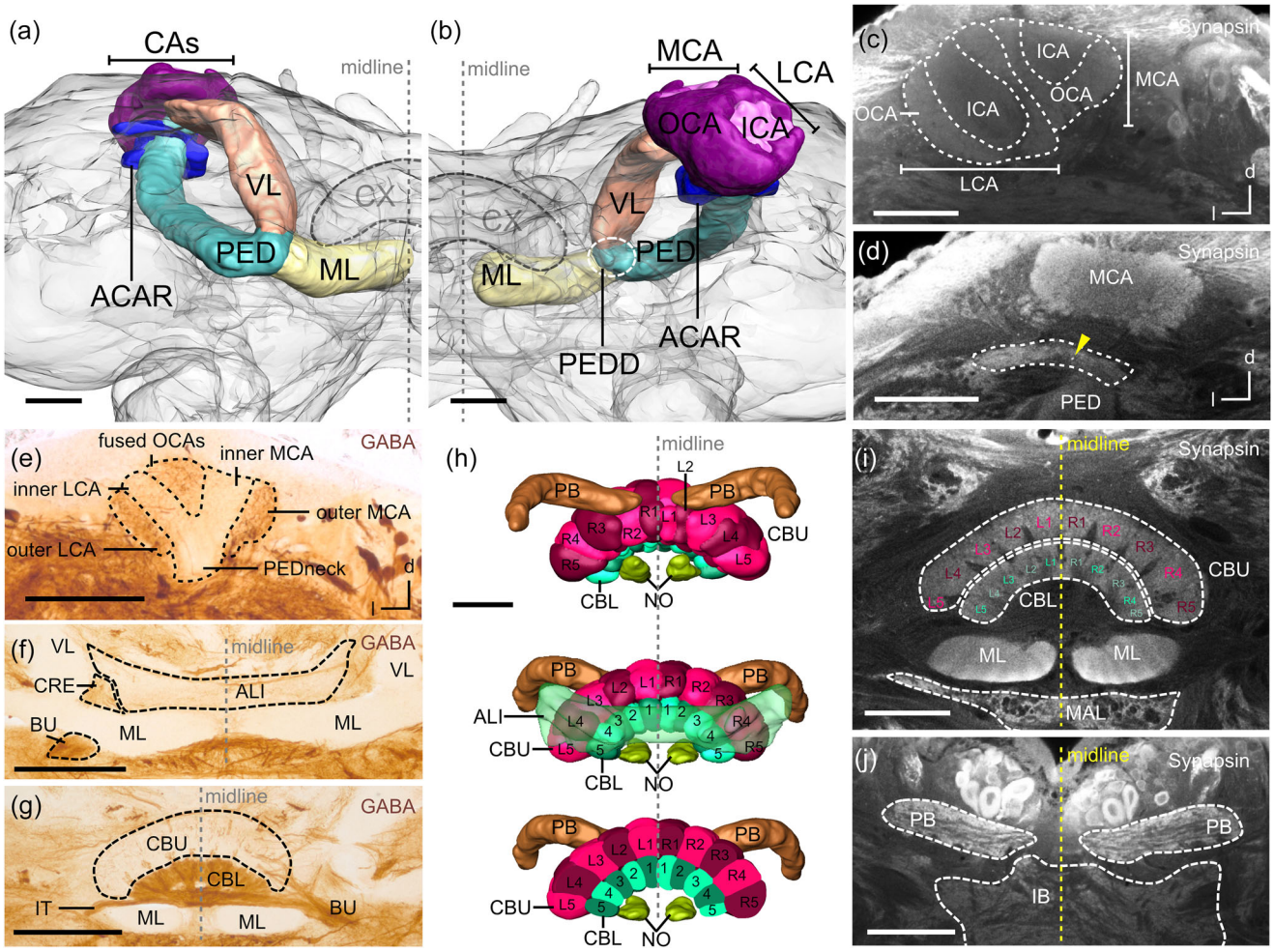

FIGURE 6 Organization of the mushroom body (MB) (a–e), central complex (CX) (g–j), and anterior lip (ALI) (f, h) in frontal views. (a, b) Three-dimensional reconstruction of the mushroom body in a semi-transparent brain hemisphere in anterior (a) and posterior (b) view. Dotted lines show the region of the pedunculus divide (PEDD). (c, d) Frontal optical sections showing synapsin immunolabeling in the calyx (CA) (c) and the accessory CA ring (ACAR). Yellow arrowhead in (d) points to accumulation of synapsin staining in the ACAR (dotted outline). (e–g) Thirty-micrometer sections immunolabeled for GABA. Dotted lines mark the borders of the CA (e), the ALI, CX, and the bulb (BU). (h) Three-dimensional reconstruction of the CX in posterior (top), anterior (middle), and anterior surface cut (bottom) views. (i, j) Frontal optical sections showing synapsin immunolabeling in the neuropils of the CX. CB, central body; CBL, lower division of the CB; CBU, upper division of the CB; CRE, crepine; d, dorsal; GABA, γ-aminobutyric acid; ICA, inner CA; IB, inferior bridge; IT, isthmus tract; l, lateral; LCA, lateral CA; MAL, medial accessory lobe; MCA, medial CA; ML, medial lobe; NO, noduli; OCA, outer CA; PB, protocerebral bridge; PED, pedunculus; VL, vertical lobe. Scale bars = 100 µm.

(Althaus et al., 2022), and the locust *S. gregaria* (Hensgen, Göthe, et al., 2021), was identified based on its strong synapsin immunolabeling, smooth and demarcated structure, and similar positioning to that observed in the other insects. The GA has a small elongated shape and lies on the ventral anterior border between the LLAL and ULAL (Figures 2b and 7c).

3.3 | SNP and lateral horn

The SLP, superior intermediate protocerebrum (SIP), SMP, anterior bridge (ABR), and the lateral horn (LH) are neuropils located in the superior protocerebrum and occupy the most dorsal parts of the mantis brain (Figures 1 and 8a).

The SLP (Figure 2b,c, 3, 4, and 5a,b) is the most lateral neuropil of the cerebrum and is through the optic stalk directly attached to the stalk lobe (SLO) of the LOX. It occupies a large volume of the dorsolateral brain region and encases dorsally the LH. The SLP extends from the superior space posterior-laterally to the SIP and laterally to the PED. Its medial boundaries include the ICL and posterior slope (PS; posterior region), as well as the SIP, SCL, and PED (anterior region). The SLP is separated ventrally from the PVLP by the LH and GC (Figure 4c). The medially lying SCL was differentiated from the SLP by numerous fibers penetrating this brain area, creating a porous appearance in synapsin immunolabeling (Figure 3). Distinguishing the SIP from the SLP was more challenging; their boundaries were set by the presence of stronger and smoother synapsin immunolabeling in the SIP compared to the SLP (Figures 2, 3, and 4a,b). The SIP (Figures 2, 3, and 4a,b)

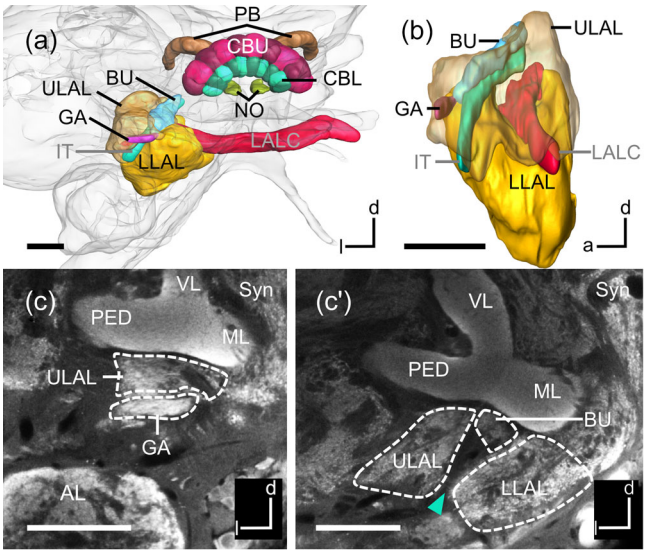

FIGURE 7 Organization of the lateral complex (LX). (a) Three-dimensional reconstruction of the LX with prominent tracts in a semi-transparent brain hemisphere, frontal view. The central complex (CX) is included for better orientation. (b) Lateral view of neuropils of the LX (labeled in black) and prominent tracts (labeled in gray). (c, c') Frontal optical sections showing synapsin immunolabeling in the LX. Dotted lines mark the neuropils of the LX and the blue arrowhead the isthmus tract (IT). a, anterior; AL, antennal lobe; BU, bulb; CB, central body; CBL, lower division of the CB; CBU, upper division of the CB; d, dorsal; GA, gall; l, lateral; LAL, lateral accessory lobe; LALC, LAL commissure; LLAL, lower LAL; m, medial; ML, medial lobe; NO, noduli; PED, pedunculus; PB, protocerebral bridge; Syn, synapsin; ULAL, upper LAL; VL, vertical lobe. Scale bars = 100 µm.

emerges anteriorly between the anterior optic tract (AOT) and AVLP and expands posterior to the AOTU. As an elongated neuropil, the SIP extends anteriorly to the mALT and CAs along the dorsal soma rind. The boundary between the SIP and the medially lying SMP was set at the level of the ascending VL (Figure 3). The distinction between the SIP, SLP, and nearby CRE was made by GABA-immunolabeled fibers that run through the SCL, targeting the CRE (Figure 9c–e). The ventral limitation of the SIP is formed by the AVLP and SCL, identifiable by strong synapsin immunolabeling of the SIP (Figure 2b,c).

The SMP was identified by its characteristic shape and its synapsin immunolabeling that is distinctive by large penetrating fibers (Figures 2b,c, 3, and 4). Unlike in the locust (von Hadeln et al., 2018) and cockroach (Althaus et al., 2022), the SMP is fused across the midline (Figure 3). It extends posteriorly to the ABR, partly surrounding the strands of the MBDL (Figure 8a). The SMP is situated medially to the SIP, medioposteriorly to the CRE, and dorsally to the ALI. It is laterally demarcated by the VLs and more posteriorly by the CAs of the MBs. The mALT defines the posterior boundary of the SMP (Figures 4c and 5a), and dorsally the SMP is bordered by the soma rind, while the fiber system around the CX and ALI covers most of its ventral face. It is attached to the SCL and ICL ventrolaterally, separated at the point where the VL ascends (Figure 4). At the dorsoanterior brain surface, the ABR, a thin neuropil, spans across the brain midline (Figures 2b,c and 8a,b). It has a grainy and fibrous structure, which is best visible in GABA immunolabeling (Figure 8b). The MBDL runs posterior from the ABR (Figure 8a). The ABR has also been identified as a distinct neuropil in the cockroach and locust (Althaus et al., 2022; von Hadeln et al., 2018), but not in holometabolous insects.

The olive-shaped LH (Figures 3b,c, 4 and 5a) protrudes laterally from the SLP toward the optic lobe (OL) and shows dense GABA immunolabeling (Figure 8c). The prominent mALT passes through the SLP, targeting the LH, thereby serving as a landmark for the identification of the LH (Figures 4c and 8d). The entire neuropil is separated from the surrounding neuropils, such as the SLP dorsally and the PVLP ventrally, by diverse fibers, clearly visible in synapsin immunolabeling and GABA immunolabeling (Figure 8c,d).

3.4 | Ventrolateral neuropils

The ventrolateral neuropils (VLNP; Figure 8e,f) comprise the VLP with an anterior (AVLP) and a posterior (PVLP) region, the posterior lateral protocerebrum (PLP), the wedge (WED), and the AOTU with a smaller lower unit (LU) and a larger upper unit (UU).

Massive fiber tracts crossing the ventral protocerebrum were used as landmarks to divide the VLP into an anterior and a posterior region (Figures 2 and 3). The AVLP (Figure 2) commences directly beneath the cell body rind and is located in the lower lateral part of the anterior brain. It touches medially the CRE and more posteriorly the PED and ULAL. Its dorsal boundaries are the SIP, SCL, and SLP, while the PVLP supersedes the AVLP at its posterior surface (Figures 3 and 8e,f). The AVLP has a denser and smoother texture (Figure 2), whereas the PVLP, the posterior part of the VLP, has a glomerular structure in synapsin staining (Figure 8h) and is heavily interspersed by fibers and large tracts (Figures 3 and 8h). Both parts of the VLP are limited by the cell body rind laterally and ventrally. The PVLP lies ventrally to the SCL, SLP, and the LH, while the PED, ICL, ULAL, and the WED adjoin medially (Figure 3). The GC marks the dorsal and posterior boundary of the PVLP to the adjacent PLP (Figures 4c, 5a, and 8e,f). The PLP in the mantis brain is relatively small and extends from the PVLP to the posterior brain surface (Figure 5a–c). It is medially limited by the lateral equatorial fascicle (LEF; Figures 5b and 8e,f), the ICL, and is more posteriorly surrounded by the PS. Dorsally, the PLP is limited by the SLP, ICL, and the lateral extension of the PS, while the WED is attached ventromedial to the PLP (Figures 5a–c and 8e,f).

One of the most ventrally lying neuropils of the protocerebrum is the WED (Figure 8e). It differs from the surrounding neuropils by its texture in synapsin immunolabeling (Figure 4) and by many tracheae and tracts that penetrate it. It is framed medially by parts of the LLAL, IFS, and the VES and is dorsally flanked by the EPA, GC, VES, and dorsoposteriorly by the PLP and PS (Figures 3b,c, 4 and 5a–c). The PVLP adjoins laterally, while the AMMC and bundles of intersegmental neurons limit the WED ventrally. It is covered posteriorly by the PS.

The AOTU is the most anterior neuropil of the protocerebrum (Figure 8e,f). It lies dorsally on the surface of the CRE (Figure 1). As in the cockroach (Althaus et al., 2022) but in contrast to the AOTU of

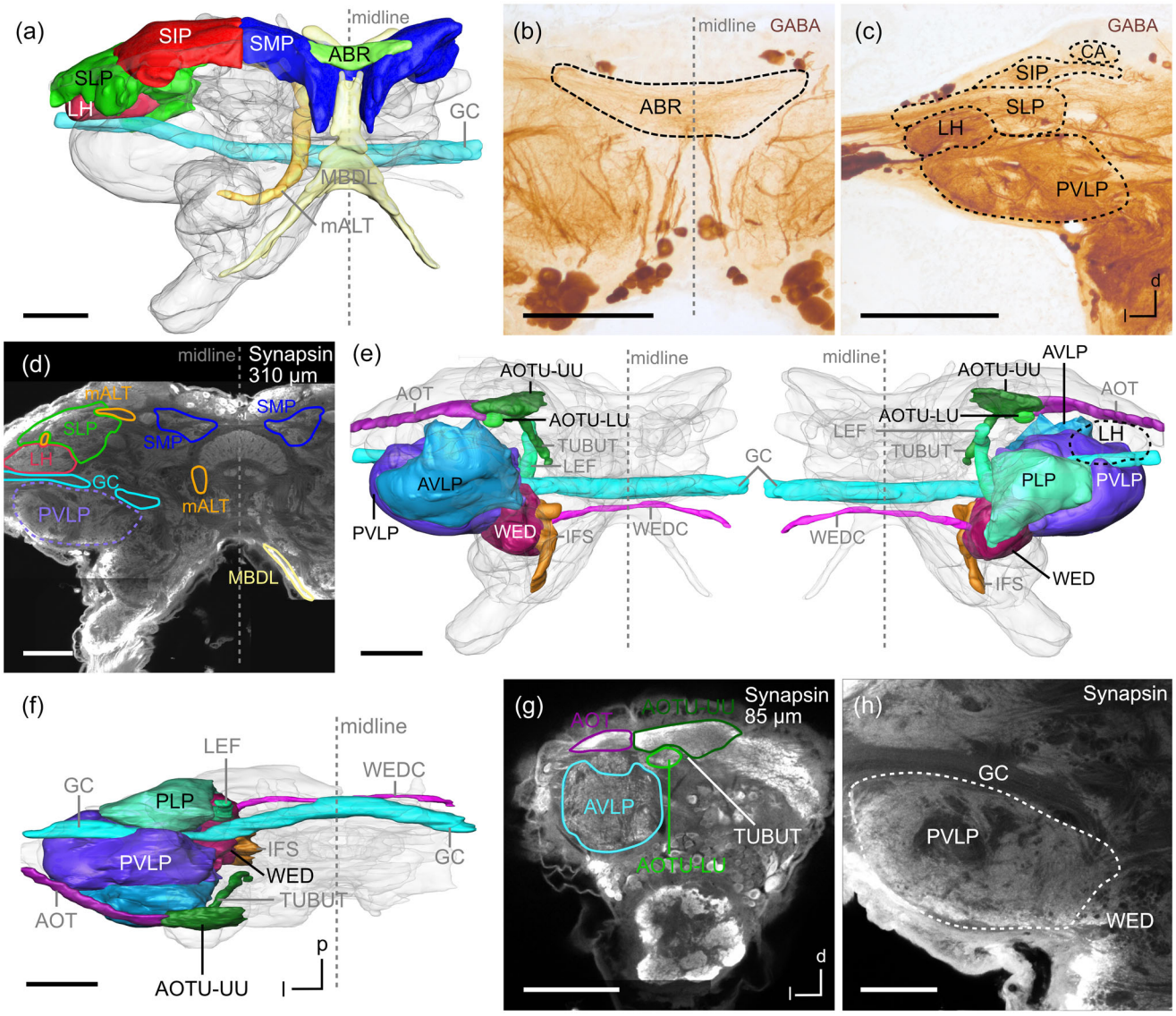

FIGURE 8 Organization of the superior (SNP) (a–d) and ventrolateral neuropils (VLNP) (e–h). (a) Anterior view of the SNP with prominent tracts in a half-transparent brain hemisphere. (b, c) Thirty-micrometer sections immunolabeled for GABA. Dotted lines mark the SNP and adjoining neuropils. (d) Frontal optical section of the synapsin-immunolabeled brain with outlines of the reconstructed label fields. (e, f) Anterior (e, left), posterior (e, right), and dorsal (f) views of the neuropils of the VLNP in a half-transparent brain hemisphere. (g) Frontal optical sections of the synapsin-immunolabeled brain with outlines of the reconstructed label fields. (h) Frontal projection view of 10 slices showing synapsin immunolabeled glomerular structures in the posterior ventrolateral protocerebrum (PVLP). ABR, anterior bridge; AOT, anterior optic tract; AOTU, anterior optic tubercle; AVLP, anterior ventrolateral protocerebrum; CA, calyx; d, dorsal; GABA, γ-aminobutyric acid; GC, great commissure; IFS, inferior fiber system; l, lateral; LH, lateral horn; LU, lower unit of the AOTU; m, medial; mALT, medial antennal lobe tract; MBDL, median bundle; LEF, lateral equatorial fascicle; p, posterior; PLP, posterior lateral protocerebrum; PVLP, posterior ventrolateral protocerebrum; SIP, superior intermediate protocerebrum; SLP, superior lateral protocerebrum; SMP, superior medial protocerebrum; TUBUT, tubercle–bulb tract; UU, upper unit of the AOTU; WED, wedge; WEDC, WED commissure. Scale bars = 200 µm (a, d–g) and 100 µm (b, c, h).

bees (Habenstein et al., 2023) and locusts (von Hadeln et al., 2018), it is relatively small. Two subunits, a larger upper unit (AOTU-UU) and a smaller lower unit (AOTU-LU), are distinguishable (Figure 8g). The AOT extends from the OL dorsolaterally along the SIP and enters the AOTU laterally. The TUBUT served to distinguish the two subunits, because it separates the UU from the LU (Figure 8g) and connects the AOTU with the BU in the LX (Figures 2 and 3a,b).

3.5 | Inferior neuropils

The INP consist of the CRE, SCL and ICL, IB, ATL, ocellar root (OR), and the MAL. In the mantis, the CRE is a flat neuropil forming the anterior surface of the brain (Figure 9a,b). The CRE lies ventral to the AOTU. The TUBUT runs through the CRE and targets the BU (Figure 2). The lateral boundaries of the CRE are demarcated by several neuropils, the AVLP,

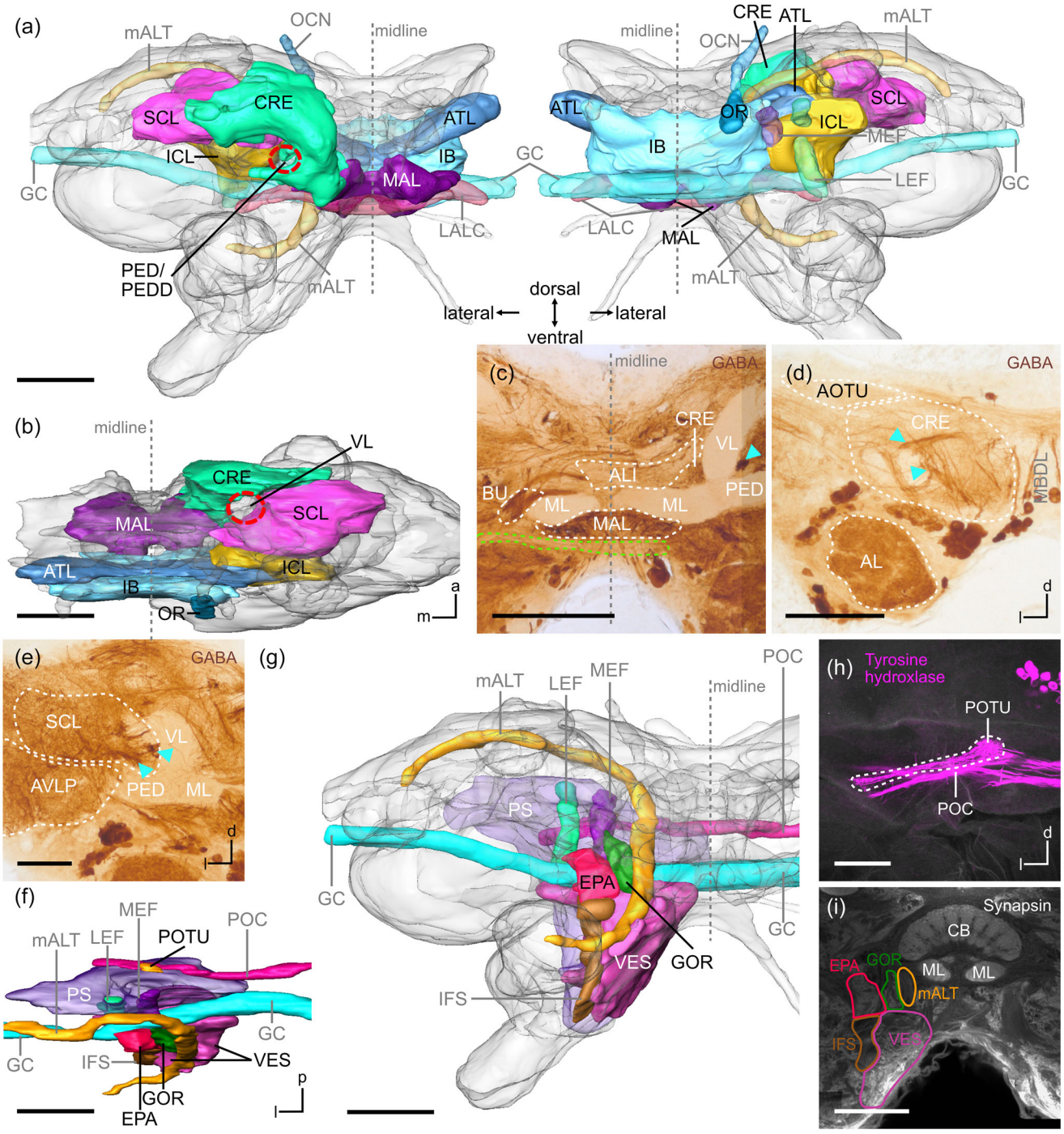

FIGURE 9 Organization of the inferior neuropils (INP) (a–e) and ventromedial neuropils (VMNP) (f–i). (a) Anterior (left) and posterior (right) view and (b) ventral view of the INP with prominent tracts (labeled in gray) in a half-transparent brain hemisphere. Red dashed circles mark the penetration of the pedunculus/pedunculus divide (PED/PEDD) in (a) and the vertical lobe (VL) in (b). (c–e) Thirty-micrometer sections immunolabeled for GABA. Dotted lines mark the neuropils of the INP and associated neuropils. (f) Dorsal view of the VMNP with prominent tracts (labeled in gray). (g) Posterior view of the reconstructed VMNP with prominent tracts (labeled in gray) in a half-transparent brain hemisphere. The posterior slope (PS) is presented semi-transparently for better visualization of the underlying neuropils. (h) Posterior projection view of 20 optical sections showing tyrosine hydroxylase (magenta) immunostaining of the posterior optic commissure (POC) and posterior optic tubercle (POTU). (i) Frontal optical section showing the reconstructed label fields of VMNP in synapsin staining. a, anterior; AL, antennal lobe; ALI, anterior lip; AOTU, anterior optic tubercle; ATL, antler; AVLP, anterior ventrolateral protocerebrum; BU, bulb; CB, central body; CRE, crepine; d, dorsal; EPA, epaulette; GABA, γ-aminobutyric acid; GC, great commissure; GOR, gorget; IB, inferior bridge; ICL, inferior clamp; IFS, inferior fiber system; l, lateral; LALC, lateral accessory lobe commissure; LEF, lateral equatorial fascicle; m, medial; MAL, medial accessory lobe; mALT, medial antennal lobe tract; MBDL, median bundle; MEF, medial equatorial fascicle; ML, medial lobe; OCN, ocellar nerve; OR, ocellar root; POC, posterior optic commissure; POTU, posterior optic tubercle; SCL, superior clamp; VES, vest. Scale bars = 200 μm (a–d, f, g, i) and 100 μm (e, h).

SIP, SCL, VL, and the PED. Medially, the SMP emerges and extends over the dorsoposterior region of the CRE (Figure 2). The posterior termination of the CRE corresponds to the level of the PEDD, except for a small protrusion between the ALI and ML (Figure 3). It almost surrounds the PEDD and ends dorsally at the ULAL (Figure 3). This bulge of the CRE is distinguishable from the ALI by GABA immunostaining, which is absent in the ALI (Figure 9c). The identification of the CRE was based on its fibrous appearance in synapsin immunolabeling and the presence of GABA-immunolabeled fibers that innervate the CRE after running through the SCL (Figure 9c–e, blue arrowheads), similar to findings in the cockroach (Althaus et al., 2022).

The MAL in the mantis is a midline-spanning neuropil (Figure 9a–c), like in the locust (von Hadeln et al., 2018). It lies ventrally to the ML and extends from the posteriorly lying IB toward the anteriorly lying CRE (Figures 3 and 4a,b). The massive LALC serves as a prominent ventral boundary of the MAL (Figure 9c). The MAL is relatively easy to identify by glomerular appearance of synapsin staining (Figures 3, 4a,b, and 6i). In contrast to the dorsally adjacent MLs, it exhibits a distinct pattern with numerous tracheae and tracts passing through it, resulting in dense perforated synapsin immunolabeling. In addition, the MAL shows strong GABA immunostaining (Figure 9c).

Another large midline-spanning neuropil of the INP is the IB covering the CB posteriorly (Figure 9a,b). Its lateral boundaries are determined by the mALT and the medial equatorial fascicle (MEF). Posterior-laterally, the IB is flanked by the ORs, which are defined as the entry neuropils of the ocellar nerves (OCNs), and the PS, distinguished by weaker synapsin immunolabeling (Figures 4a and 5a–c). The OR extends from the OCN posteriorly and curves medially to the posterior bend of the PB (Figure 5c). The anterior surface of the IB is attached to the MAL (Figure 4b,c), and the dorsoanterior side is covered by the ATL that spreads over the entire surface of the IB (Figure 9a,b). Further posteriorly, the fiber system space below the PB serves as the dorsal boundary of the IB (Figure 5b). Ventrally, the IB is mainly framed by the GC (Figure 5a–c) and, more anteriorly, by another large undefined commissure and the VES (Figure 4c).

As mentioned above, the ATL extends along the dorsal surface of the IB and is, thus, the third midline-spanning neuropil of the INP. It is positioned ventroposteriorly to the CB (Figure 4c). The ATL extends from the midline into both hemispheres and has a club-like shape (Figure 5a). It is dorsally framed by the mALT and ventrally by the ICL and MEF (Figure 5a). The posterior part of the ATL is superseded by the PS and IB (Figure 5a,b).

The most inferior region of the hemispheres is occupied by the clamp (CL). Similar to the locust and cockroach (Althaus et al., 2022; von Hadeln et al., 2018), the ascending PED serves as a boundary between the two subdivisions of the CL (Figure 3), the SCL and ICL (Figure 9b). The latter is positioned anterior to the PS, separated from it by the LEF (Figure 5a,b). Posterior medial boundaries are defined by the MEF, while the anterior medial boundaries are formed by the IB, ATL, and the fiber system around the CX. Laterally, the ascending PED limits the ICL, and its ventral borders are marked by the ULAL, EPA, gorget (GOR), GC, and PVLP/PLP (Figures 4 and 5a). The area located anteriorly to the PED and laterally to the VL is defined as the SCL (Figures 2, 3, and 4a,b). The SCL lies anteriorly between the CRE, the SIP, and the AVLP. In the more posterior part, the SCL is encased by the SIP/VL/SMP (dorsally), the CX/ICL/VL (medially), the SLP (laterally), and the PED and PVLP (ventrally). GABA-immunolabeled fibers run through the SCL along the lateral face of the VL and target the CRE (Figure 9c–e, blue arrowheads).

3.6 | Ventromedial neuropils

The ventromedial neuropils (VMNP) are located posterior and inferior to the AL. This group of neuropils in the ventromedial cerebrum includes the EPA, GOR, VES, PS, and the posterior optic tubercle (POTU).

The POTU was identified by synapsin immunolabeling and more clearly by TH immunolabeling at the posterior surface of the mantis brain (Figure 9h). It lies posterior from the PS and is dorsally attached to the posterior optic commissure (POC; Figures 5d and 9h). The EPA, GOR, and VES comprise the ventral complex (VX), with the VES being the largest in volume (Figure 9g). The VES (Figures 4, 5a–c, and 9g,i) extends along the esophageal passage posterior to the mALT. Its lateral boundaries are defined by the IFS, LLAL, EPA, and WED. Ventrally, the boundary is formed by the AMMC, while the dorsoanterior boundary is marked by the MAL and EPA. Its dorsoposterior limitation is set by the GC (Figure 5a,b). The posterior surface of the VES is covered by the PS, and the WED commissure (WEDC) serves as a significant landmark for distinguishing PS and VES (Figure 5c).

The other VX-associated neuropils, the EPA and GOR, are significantly smaller in size. The GOR (Figures 4b and 9f,g,i) is attached dorsally to the VES and has been described in *D. melanogaster* as an extension of the VES (Ito et al., 2014). In the mantis brain, it protrudes lateral to the mALT, corresponding to the GOR in the cockroach (Althaus et al., 2022). It is characterized by its conspicuous porous synapsin immunolabeling and the presence of surrounding tracts (Figures 4b and 9i). The GOR ascends toward the ICL and is laterally limited by the EPA. The EPA (Figures 4b and 9f,g,i) lies dorsolaterally from the VES. It lies anterior to the GC and posterior to the ULAL. The EPA serves as a "connection" between the VES and ICL, similar to its description in the fruit fly (Ito et al., 2014).

In addition to the VX, the PS (Figures 5b–f and 9f,g) is also part of the VMNP. It occupies a large volume and covers most parts of the posterior surface of the brain. The PS is located posterior to the GC and may be further divided into a superior and inferior PS as described in the fruit fly, where both are divided by the POC (Ito et al., 2014). However, in the mantis, no subdivisions of the PS were recognized, so that it is considered as a single unit.

3.7 | AL and PENP

The AL occupies a position ventral from the LX and the VMNP and covers the PENP anteriorly (Figures 2 and 3). It consists of about 61 olfactory glomeruli that exhibit dense synapsin labeling. The glomeruli

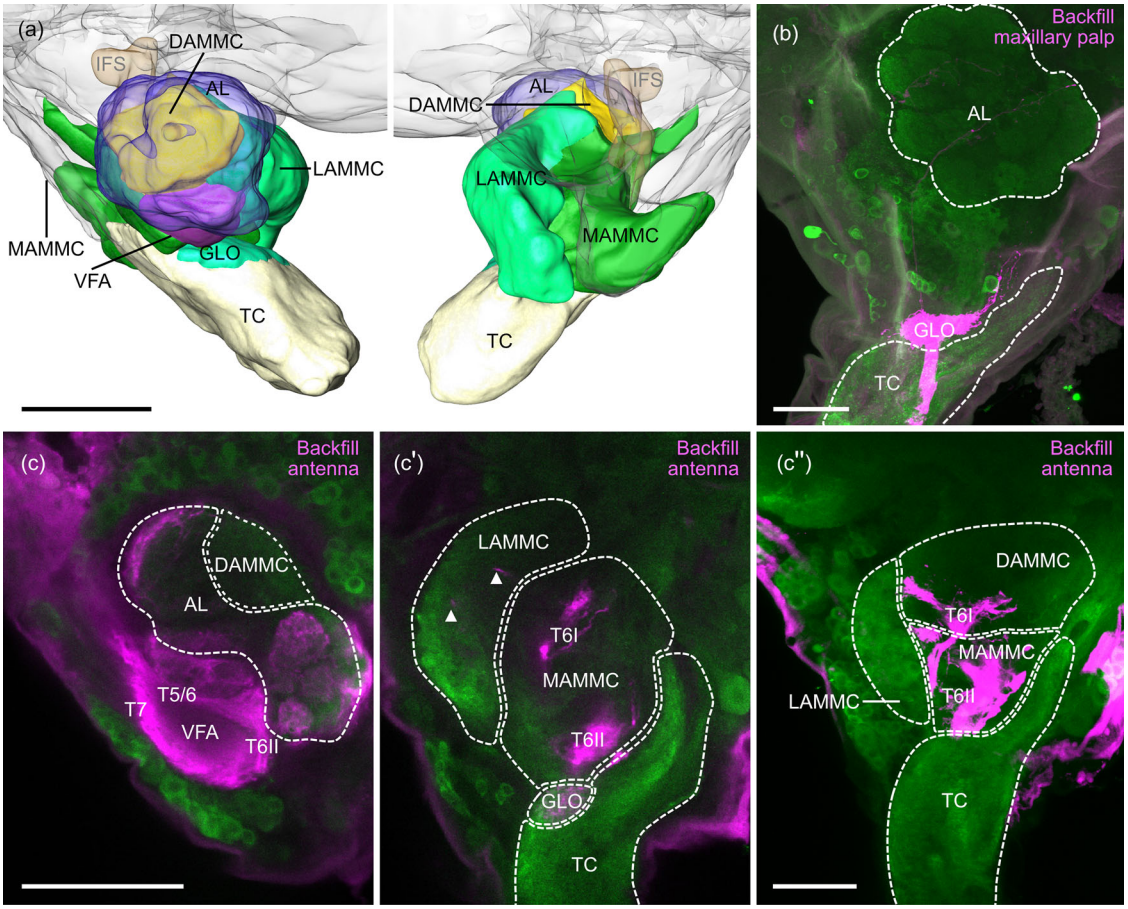

FIGURE 10 Organization of the antennal lobe (AL), the periesophageal neuropils (PENP), and the tritocerebrum (TC). (a) Anterior (left) and posterior (right) views of the reconstructed neuropils in a semi-transparent brain hemisphere. The AL and the inferior fiber system (IFS) are, likewise, displayed half-transparently for better visualization of the adjoining neuropils. (b) Projection view of a stack of 190 labeled sections showing a backfill of the maxillary nerve from the maxillary palp (magenta). (c, c') Single frontal optical sections showing the PENP following a backfill of the antennal nerve from the flagellum of the antenna. (c'') Projection view of a stack of 70 optical sections showing the projections of antennal afferents revealed by a backfill of the antennal nerve from the scapus–pedicel joint (magenta). AMMC, antennal mechanosensory and motor center; DAMMC, dorsal AMMC; GLO, glomerular lobe; LAMMC, lateral AMMC; MAMMC, medial AMMC; T5–7, tract 5–7; TC, tritocerebrum; VFA, ventral area of flagellar afferents. Scale bars = 200 μm (a) and 100 μm (b–c'').

are largely arranged along the periphery of the AL, while the center of the AL, the antennal lobe hub, consisting of fibers of projection and local neurons, shows considerably lower levels of synapsin staining (Figure 2a). Surrounded by extensive glial sheaths, the AL is clearly distinguishable from adjacent brain areas. The PENP are located posterior to the AL and comprise the strongly interconnected AMMC subunits and the glomerular lobe (GLO) and the more ventrally lying tritocerebrum (TC) that is positioned most ventrally within the cerebral ganglia (Figure 10a).

The AMMC is the most voluminous area of deutocerebral origin and is subdivided into four units: the dorsal AMMC (DAMMC), the lateral AMMC (LAMMC), the medial AMMC (MAMMC), and the ventral area of flagellar afferents (VFA). Originating in the AL, the mALT sets the anterior border of the DAMMC that follows the AL posteriorly (Figures 3a,b and 10a). The VFA lies at its ventral border, while the DAMMC adjoins the ULAL ventrally. The LAMMC (Figures 3, 4, 5a, and 10a,c',c'') lies posterior-laterally from the DAMMC and is characterized by its hill-like bulge that protrudes laterally toward the cell cortex. It is ventrally bound by the VFA, GLO, and TC and bordered dorsally by the WED and LLAL. The LAMMC is surrounded by massive intersegmental fibers in medioposterior direction, and the majority of its medial parts are covered by the MAMMC. The third area of the AMMC, the MAMMC, borders on a medial soma cluster along the esophageal foramen, lies ventroposterior to the DAMMC, and touches the WED, LLAL, and the VES mediodorsally (Figures 3, 4, 5a, and 10a,c',c''). It is ventrally limited by the GLO and the TC, and its most posterior region is surrounded by fibers of the circumesophageal connective. The last unit of the AMMC, the VFA (Figures 2c, 3a,b, and 10c), adjoins the AL at its posterior face and is enclosed by the compartments of the AMMC. It is located dorsally to the GLO. Its identification is based on backfills from the antennal flagellum (Figure 10c). It receives innervation from flagellar afferents, clearly differentiating it from surrounding areas. Mechanosensory afferents labeled by antennal backfills split into several tracts and fascicles, corresponding to

tracts T5–T7 in the cricket (Staudacher & Schildberger, 2000). Tract 5/6 terminates in the AMMC, previously called dorsal lobe, and splits into two strands, T6I and T6II. T6I spreads into the MAMMC with two strings running into parts of the LAMMC (Figure 10c', white arrowheads) and ventral parts of the DAMMC (Figure 10c''). In contrast, T6II runs more ventrally with projections in the MAMMC (Figure 10c',c'') and further projects ventrally into the pharyngeal connectives. Tract T7 projects into the VFA (Figure 10c).

The TC, the most ventral neuropil of the mantis brain (Figures 3, 4 and 10a,b), was clearly discernible by synapsin immunostaining. A granular region appears ventrally to the AL, embedded in the dorsal region of the TC, and extends further posteriorly. This texture is characteristic for the GLO. The identification of the GLO by synapsin immunolabeling in the mantis brain was challenging (Figures 3b,c and 4a,b). It is less distinctive than in the cockroach, where it is a prominent glomerular neuropil (Althaus et al., 2022). Therefore, we confirmed its presence by backfills from the ipsilateral maxillary palp. The GLO was strongly stained by backfilled maxillary afferents (Figure 10b), enabling clear differentiation for the 3D reconstruction.

3.8 | Tracts and commissures

We identified and reconstructed 12 fiber tracts, fiber systems, and commissures (Figure 1) that served as landmarks in the mantis brain. They were determined based on the absence of synapsin labeling in the wholemount preparation.

The mALT is one of the most prominent tracts (Figures 3 and 4). It originates in the AL and runs dorsally between the AMMC and LLAL. It then continues medially between the LLAL and VES/MAL. Along the lateral CX, the mALT extends dorsally and protrudes laterally along the dorsal surface of the ATL. It bypasses the PED anteriorly, runs through the SLP, and targets the LH from dorsal direction. Another easily identifiable tract is the IT (Figure 3a,b), characterized by strong GABA immunostaining (Figure 6g). The IT contains numerous neurons connecting the LX to the CX. These include many GABA-labeled tangential neurons arborizing in the CBL and BU with somata in a cluster near the AL (Homberg et al., 2018). The IT serves to differentiate the ULAL and LLAL, similar to the LALC. Two tracts associated with the AOTU are the AOT and the TUBUT (Figures 2 and 3a,b). The AOT connects the optic lobe with the AOTU. It runs along the anterior face of the SLP and SIP. Its identification, along with the TUBUT, was essential for recognizing the AOTU. The TUBUT originates between the lower and upper units of the AOTU (Figure 8g) and establishes connections with the BU. It runs from the AOTU through the CRE, along the medial border of the SCL, to the BU and delineates the boundary between the SCL and ULAL/BU (Figure 3a,b). The OCNs (Figures 4c and 5a–c) were easy to identify, as they comprise the neurites of ocellar interneurons. These neurons enter the brain from dorsal direction, bypass the PB posteriorly, and target the OR.

Two prominent fascicles that were identified in the mantis brain are the LEF and MEF, both located in the posterior protocerebrum. The LEF (Figure 5a,b) emerges from the GC between the ICL and VES and runs dorsally through the ICL, extending further posteriorly through the dorsal area of the PS. The MEF (Figure 5a–c) is positioned more medially than the LEF. It extends from the posterior tip of the PB ventrally toward the GC, forming the lateral boundary of the IB. Another dominant tract is the MBDL (Figures 2c, 3 and 4a,b). It contains fibers of neurosecretory cells of the pars intercerebralis, among others, and extends along the anterior midline of the brain. Ventral to the MAL, it splits into two fiber bundles that continue their ventral course along the lateral sides of the esophagus before many of its fibers enter the corpora cardiaca nerve. The MBDL marks the posterior borders of the ABR and SMP.

In the fruit fly, two major fiber systems, the IFS and superior fiber system (SFS), were used for identifying neuropil boundaries. In the mantis brain, we could only identify the IFS, as the SFS is not as prominent as in the fruit fly or the Madeira cockroach. The IFS is a fiber system in the ventral brain region, lying between the VES and WED, which limits the LAL posteriorly (Figure 4a,b).

We identified four commissures that cross the midline of the mantis brain. These commissures primarily connect bilateral neuropils of both brain hemispheres. Notably, the GC and LALC stand out due to their large size. The LALC (Figures 3b,c and 4a,b) connects the right and left LAL, and served as the boundary between the ULAL and LLAL, along with the IT. Moreover, the LALC forms the ventral border of the MAL as it crosses the brain midline. The GC (Figures 4c and 5a–c) connects both OLs with each other. It was used for the separation of the LH and PVLP, as well as PVLP and PLP. It also defined the border between the ICL and the VES. While crossing the brain midline, the GC also sets the ventral border of the IB. The POC runs along the dorsoposterior brain surface, between the PS and the POTU (Figure 5d). It connects both optic lobes with each other and contains TH-immunoreactive neurons that innervate the POTU (Figure 9h). Lastly, we identified the WEDC (Figure 5b,c), which connects the two WEDs with each other. The WEDC helped in determining the boundaries of the WED and partly served as the border between the VES and PS.

3.9 | Anatomical organization of optic lobe neurons

To demonstrate the usefulness of the atlas for the analysis of the location of neuronal arborizations in the mantis brain, we integrated seven intracellularly recorded neurons of the optic lobes into the 3D atlas. The cells were published by Rosner et al. (2019, 2020) and comprise four projection neurons (TOpro1, TOpro2, TApro$_{prox}$1, and TAOpro), two centrifugal neurons (TAcen and TMEcen), and a commissural neuron (COcom) interconnecting both optic lobes. We list the ramification sites of these neurons in Table 1. Additionally, we scrutinized the branching areas of the remaining types of neurons published by Rosner at al. (2019, 2020) and took into account the insights from this study about neuropil locations within the central brain. We provide the updated information about the ramification sites of these cells in Table 1 as well.

TABLE 1 Ramification areas of visual interneurons in the mantis described in Rosner et al. (2019, 2020).

			Ramification areas within the OL						Ramification areas within the central brain											
Neuron	ID[1,2]	Fig.	ME	ALO-D	ALO-P	DLO	OLO	SLO	AMMC	AVLP	EPA	GOR	ICL	LAL	PLP	PVLP	PS	SLP	VES	WED
TOpro1	160125[2]	2a					x				x				x	x	x		x	x
TOpro2	160301[2]	2c					x			x					x	x				
TApro$_{prox}$1	151013[2]	4a			x					x				x					x	x
COcom	151123[1]	3					x								x	x				x
TAOpro	160427[1]	1c		x			x								x	x			x	
TAcen	170606[1]	4a,b		x					x						x		x			x
TMEcen	161025[1]	4c–e	x									x			x		x		x	x
TOpro3	160503[2]	2d					x			x					x	x				
TApro$_{prox}$2	151102[2]	4d			x							x			x	x	x	x	x	x
TApro$_{prox}$3	170629[2]	4e			x								x		x	x	x	x		
Spro	170203[2]	4f						x		x						x				
TMeASpro	170605[2]	5b	x					x										x		
TMeOSpro	160216[2]	5a	x				x	x							x	x			x	x
TApro$_{dist}$1	151111[2]	3e		x											x		x			x
TADpro	161115[2]	3b		x		x								x	x		x			x

Note: Figure numbers (Fig.) and identification numbers (ID[1,2]) refer to Rosner et al. (2019)[1] and Rosner et al. (2020)[2]. The upper box shows neurons registered here, while the lower box lists the remaining types from Rosner et al. (2019, 2020). All neurons were studied in *Hierodula membranacea*, except TApro$_{prox}$3 (*Hierodula unimaculata*) and TADpro (*Rhombodera megaera*). The presence of arborizations is indicted by an x. Abbreviations: ALO, anterior lobe of the lobula complex; ALO-D, distal ALO; ALO-P, proximal ALO; AMMC, antennal mechanosensory and motor center; AVLP, anterior ventrolateral protocerebrum; DLO, dorsal lobe of the lobula complex; EPA, epaulette; GOR, gorget; ICL, inferior clamp; LAL, lateral accessory lobe; ME, medulla; OLO, outer lobe of the lobula complex; PLP, posterior lateral protocerebrum; PVLP, posterior ventrolateral protocerebrum; PS, posterior slope; SLO, stalk lobe of the lobula complex; SLP, superior lateral protocerebrum; VES, vest; WED, wedge.

The TOpro1 and 2 neurons are tangential projection neurons with input in the outer lobes (OLOs) 1 and 2 of the LOX (Rosner et al., 2020). The soma of TOpro1 is located in the OL, specifically in the dorsoanterior region near the SLO. The cell body fiber runs ventrally through the "tunnel" of the SLO and connects to the main neurite (Rosner et al., 2020). This main neurite enters the brain through the GC and has widely spread beaded arborization in several neuropils in the ipsilateral brain, including the PLP, PS, WED, EPA, and the dorsal region of the VES (Figure 11a,b''). The innervation of the transition area from the PVLP to the PLP (Figure 11b'; small area above the GC) is particularly noteworthy, as this area is also innervated by the TOpro2 and COcom neurons. The axon of the TOpro2 runs along the ventral part of the GC and gives rise to beaded projections in the PVLP and PLP of the ipsilateral hemisphere of the brain (Figure 11c,d), as well as in the transition area from the PLP to the PVLP (Figure 11c).

The TAPro$_{prox}$1 neuron ramifies in proximal parts of the ventral lobe of the anterior lobe of the lobula complex (ALO; Rosner et al., 2020) and has axonal terminals in the ipsilateral protocerebrum. The soma of the TAPro$_{prox}$1 is located in the soma rind near the PVLP (Rosner et al., 2020; Figure 12b''). From the OL, the main neurite runs anteriorly through the AOT. It enters the AVLP and gives off small, beaded processes in the anterior shell of the AVLP (Figure 12a,b'). The neurite continues posteriorly, makes a ventral turn, and sends side branches into anterior parts of the LLAL and small, beaded branches into the anterior ULAL. Wide arborizations are finally concentrated in the VES and WED (Figure 12a,b'). The TAOpro neuron is a tangential projection neuron with dendrites in OLO1/2 and in the distal layer of the ALO and axonal terminals in the ipsilateral protocerebrum. Its soma is located posterior to the SLO (Rosner et al., 2019; Figure 12c,d'). The main neurite runs from the OL through the GC into the central brain. The neuron shows sparse ramifications in the PLP and PVLP, as well as in the transition area of the PLP and PVLP dorsal to the GC (Figure 12d), like the TOpro1 and 2 neurons. The TAOpro neuron continues from the GC into the IFS along the lateral side of the VES, with two fine branches that innervate the VES (Figure 12c,d).

The COcom neuron is a commissural neuron connecting the OLO1/2 of both optic lobes. Its main neurite runs along the GC and has mirrored ramifications in both hemispheres of the central brain, but differs in the optic lobes. The neuron has smooth ramification in the OL ipsilateral to the soma (input) and beaded endings in the contralateral OL (output). The arborizations, from lateral to medial, invade the transition area from the PLP to the PVLP (adjacent dorsally to the GC), the PLP, the WED, and the VES with bleb-like endings (Figure 13a,b'). The TAcen neuron is a tangential centrifugal neuron with broad ramifications in the distal parts of the ALO (Rosner et al., 2019; Figure 14a,b). The soma of this neuron is located near the ventromedial edge of the AVLP. The cell body fiber enters the protocerebrum posteriorly, runs along the dorsoanterior surface of the PLP, and then continues in anteromedial direction. Sparse fine side branches are given off into the DAMMC and MAMMC, while the main second neurite runs through the WED and sends a side branch posteriorly into the PLP and PS (Figure 14a,b) before it continues dorsolateral to the PLP in the optic stalk. The TMEcen neuron is a tangential centrifugal neuron with wide ramifications across the contralateral ME (Rosner et al., 2019; Figure 14d). Its soma is located in the posterior soma rind of the central brain. The neuron ramifies bilaterally in the central brain (Figure 14d'). Ipsilateral ramifications are in the posterior lateral VES, from which the main neurite crosses the midline posteriorly. It further exhibits contralateral processes in the PS, VES, WED, PLP, and a small branch projecting into the GOR (Figure 14c,d').

4 | DISCUSSION

We have analyzed and reconstructed a total of 42 neuropils and 12 tracts and commissures of the cerebrum of the mantis *H. membranacea*, in addition to the seven reconstructed neuropils of the mantis OL presented by Rosner et al. (2017). This opens up new possibilities for detailed anatomical analysis. Therefore, we integrated seven 3D-reconstructed neurons published in Rosner et al. (2019, 2020) into the 3D atlas, allowing for detailed identification of their arborization areas in the central brain (Figure 15). This provides a basis for mapping neuronal connections in future anatomical and physiological studies. We found prominent, strongly innervated neuropils, including the PLP, PVLP, as well as the WED and VES targeted by the optic lobe neurons. The GC is strikingly prominent in the mantis brain, potentially serving binocular computations. Brain areas, such as the ALI, ABR, and MAL, present in the mantis brain, seem to be unique in polyneopteran insects (cockroach [*R. maderae*] and locust [*S. gregaria*]). However, a correspondence of the neck, identified in the locust and cockroach, was not found in the mantis brain. The MB of the mantis appears relatively slim compared to the MB of the cockroach and locust. Other chemosensory neuropils such as the GLO and AL are, likewise, less prominent, while visual neuropils of the OL are large and partitioned in a highly complex manner in the mantis brain. This is likely due to the mantis' strong reliance on visual input.

4.1 | Mushroom body

The CAs vary in number and complexity across different insect species and, in aquatic species, may be completely absent (Strausfeld et al., 2009). Our findings in the mantis support the previously described fused double cup organization of the CA (Rosner et al., 2017) and unveil the presence of an ICA and OCA within each CA. In addition, an ACAR encircling the PED neck of the MB is present. As demonstrated in various insects, like the honey bee *A. mellifera*, the cockroach *P. americana*, and the fly *D. melanogaster*, the MBs are strongly involved in learning, memory, and integration of multisensory, in particular olfactory, inputs (Heisenberg, 1998; Li et al., 2020; Menzel, 2022; Mizunami et al., 1998; Modi et al., 2020; Nishino et al., 2012). The MBs in the mantis have relatively slender dimensions, in contrast to their counterparts in the cockroach (Althaus et al., 2022, Wei et al., 2010), locust (Kurylas et al., 2008; von Hadeln et al., 2018), or honey bee (Strausfeld, 2002). This difference may be related to the ecology of mantises, which rely mainly on visual input, rather than olfaction.

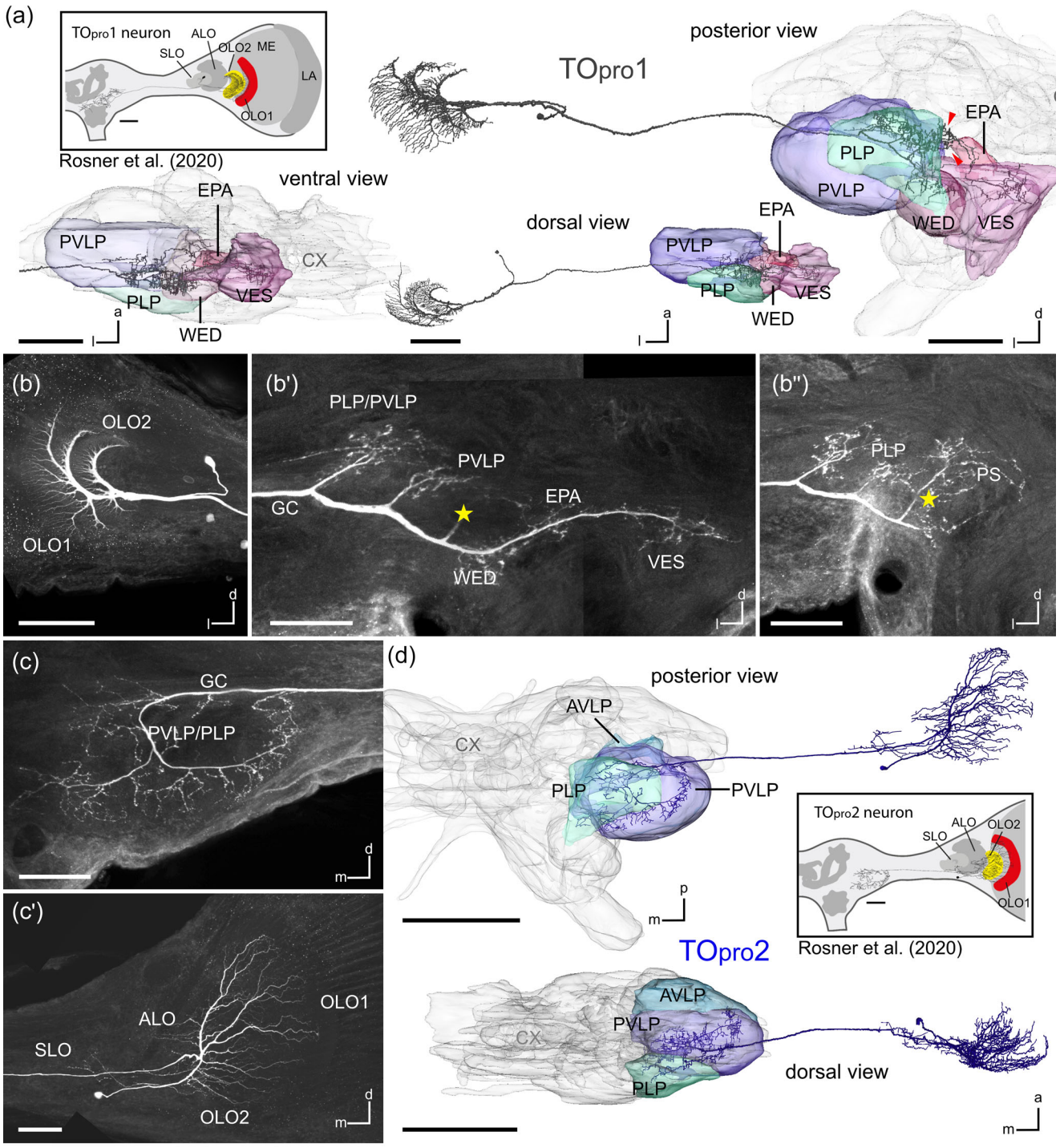

FIGURE 11 Three-dimensional reconstructions of the TOpro1 and TOpro2 neurons (Rosner et al., 2020) integrated into the 3D atlas of the mantis brain. (a) TOpro1 neuron integrated into the half-transparent 3D atlas, showing innervated, colored neuropils in posterior (right), dorsal (middle), and ventral views (left bottom). Red arrowheads point to arborizations in the posterior slope (PS). Inset (top left) shows the reconstructed neuron from Rosner et al. (2020) with innervated neuropils of the optic lobe. (b–b'') Anterior projection view of 100 slices (b), 115 slices (b'), and 25 slices (b'') of the Neurobiotin-injected TOpro1 neuron. Yellow asterisk marks the connection to the posterior ramifications of the neuron (b''). It arborizes widely in the outer lobe of the lobula complex (OLO) and enters the cerebrum via the great commissure (GC). The neuron has wide arborizations in the ipsilateral brain hemisphere. (c, c') Projection view of 120 slices of the Neurobiotin-injected TOpro2 neuron in the ipsilateral cerebrum (c) and of 120 slices of the optic lobe (c'). The neuron has wide arborizations in the OLO, anterior lobe of the lobula complex (ALO), and the stalk lobe of the lobula complex (SLO), anterior view. (d) TOpro2 neuron integrated into the 3D brain atlas with innervated neuropils highlighted in color in posterior (top) and dorsal views (bottom). Inset shows image of the reconstructed neuron from Rosner et al. (2020) with the innervated areas in the optic lobe (right middle). a, anterior; AVLP, anterior ventrolateral protocerebrum; CX, central complex; d, dorsal; EPA, epaulette; l, lateral; LA, lamina; m, medial; ME, medulla; OL, optic lobe; PLP, posterior lateral protocerebrum; PVLP, posterior ventrolateral protocerebrum; VES, vest; WED, wedge. Scale bars = 200 µm (a, b), 100 µm (b'–c'), and 400 µm (d).

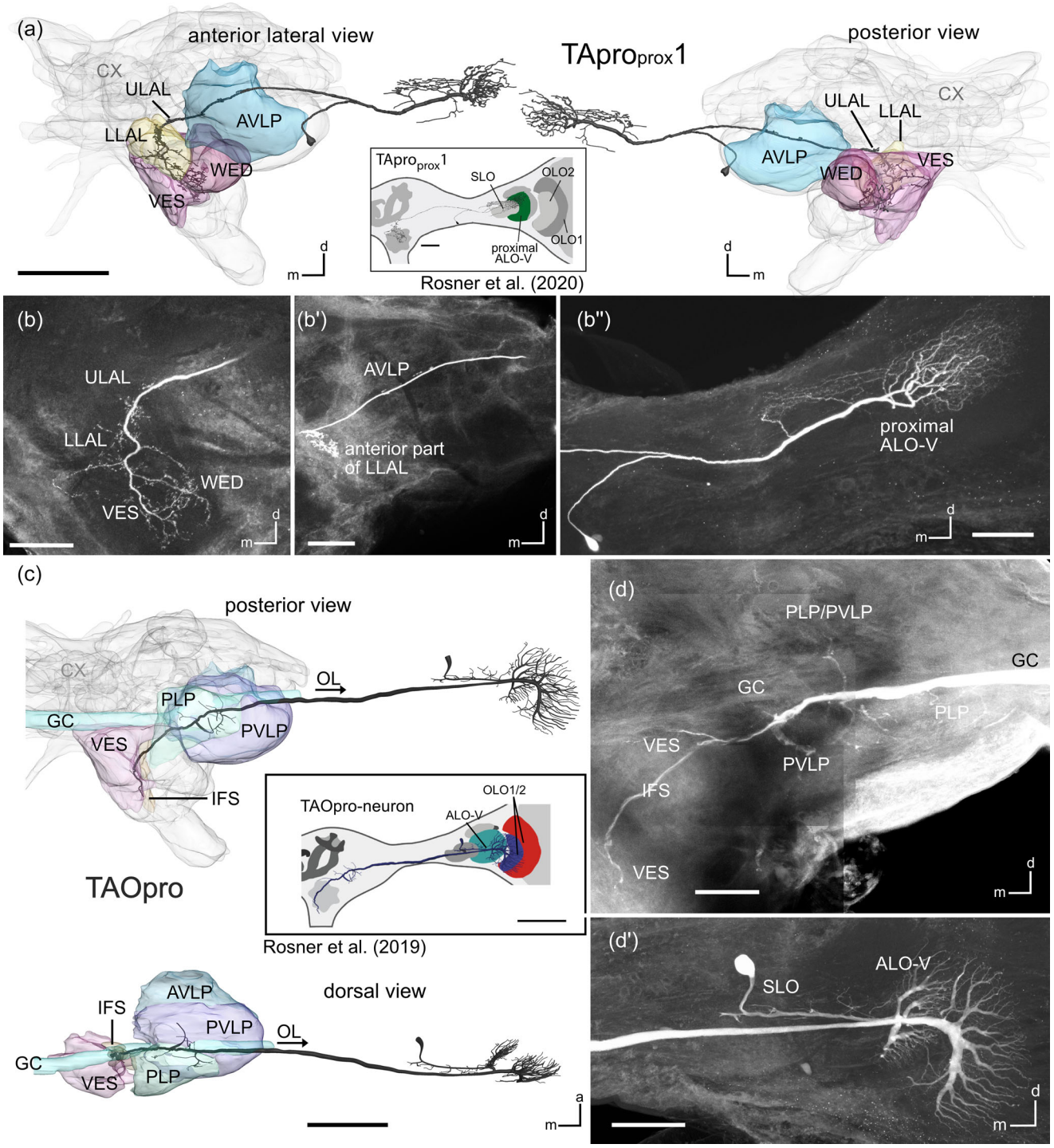

FIGURE 12 Three-dimensional reconstructions of the TAPro$_{prox}$1 (Rosner et al., 2020) and TAOpro neurons (Rosner et al., 2019). (a) Three-dimensional reconstruction of the TAPro$_{prox}$1 neuron integrated into the half-transparent 3D atlas with colored innervated neuropils in posterior (right) and anterior lateral views (left). Inset shows neuron from Rosner et al. (2020) in anterior view with innervated areas of the optic lobe (middle). (b–b") Anterior projection views from posterior (130 slices in b) to anterior (50 slices in b' and 60 slices in b"). (c) Three-dimensional reconstruction of the TAOpro neuron integrated into the half-transparent 3D atlas with innervated neuropils and the great commissure (GC) in colors, posterior (top) and dorsal (bottom) views. Inset shows neuron from Rosner et al. (2019) in anterior view with innervated areas of the optic lobe (OL). (d, d') Anterior projection view of the Neurobiotin-injected TAOpro neuron from 80 slices of the central brain (d) and 60 slices of the OL (d'). a, anterior; ALO, anterior lobe of the lobula complex; ALO-V, ventral ALO; AVLP, anterior ventrolateral protocerebrum; CX, central complex; d, dorsal; IFS, inferior fiber system; l, lateral; LLAL, lower lateral accessory lobe; m, medial; OLO, outer lobe of the lobula complex; PLP, posterior lateral protocerebrum; PVLP, posterior ventrolateral protocerebrum; SLO, stalk lobe of the lobula complex; ULAL, upper lateral accessory lobe; VES, vest; WED, wedge. Scale bars = 200 µm (a), 100 µm (b, b', b", d), 200 µm (d'), and 300 µm (c).

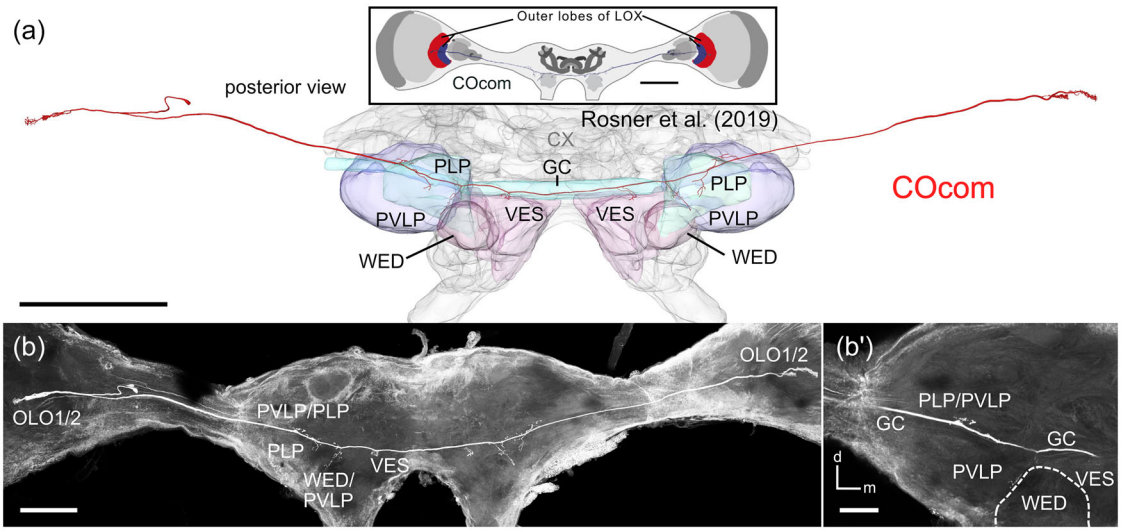

FIGURE 13 (a) Three-dimensional reconstruction of the COcom neuron (Rosner et al., 2019) integrated into the half-transparent 3D atlas with innervated neuropils and the great commissure (GC) in colors, posterior view. Inset shows neuron from Rosner et al. (2019) in anterior view with innervated areas of the optic lobes (OLs). (b, b') Anterior projection view of the Neurobiotin-injected COcom neuron from 70 slices of the whole neuron (b) and 20 slices of the arborization in the transition area from the posterior lateral protocerebrum (PLP) to the posterior ventrolateral protocerebrum (PVLP) (b'). CX, central complex; d, dorsal; m, medial; OLO, outer lobe of the lobula complex; VES, vest; WED, wedge. Scale bars = 500 μm (a), 600 μm (b), and 200 μm (b').

4.2 | CX, ALI, and LX

The CX is a structure highly conserved across insect species. In the mantis, both divisions of the CB are divided into 10 vertical slices (five per hemisphere). Their shape can be described as wedge-like, similar to the teeth in the CBL of the cockroach (*R. maderae*) (Althaus et al., 2022; Jahn et al., 2023). The outer slice of the CBL was previously described as half-sized (Rosner et al., 2017), which is consistent with our observations. The CX is strongly involved in controlling spatial behavior and processing of navigational information. It receives input from various sensory sources, including various visual and antennal mechanosensory cues (Honkanen et al., 2019; Pfeiffer, 2022; Pfeiffer & Homberg, 2014). Extracellular recordings in the freely moving Chinese mantis (*Tenodera sinensis*) suggest that CX neurons are involved in prey detection and tracking (Wosnitza et al., 2022). The ALI, covering the CB frontally, has been identified as a CX-associated neuropil in the cockroach (Althaus et al., 2022; Jahn et al., 2023), locust (Heinze & Homberg, 2008; Vitzthum et al., 1996), and honey bee (Hensgen, England, et al., 2021). In the polyneopteran species, the ALI is large; it is considerably smaller in bees and not present as a distinct neuropil in fruit flies (Ito et al., 2014).

The neuropils of the LX are closely linked with the CX and serve as an input and output site for various information to and from the CX (Hensgen, Göthe, et al., 2021; Hulse et al., 2021; Pfeiffer & Homberg, 2014). In the mantis, the LX is largely unexplored, but we discovered input from optic lobe neurons (TApro$_{prox}$1, TADpro; Table 1). In the fruit fly (*D. melanogaster*), descending neurons convey information from the LAL downstream to regions involved in motor control (Namiki, Dickinson, et al., 2018) that may be similar in the mantis. The microglomerular organization of the BU in the mantis is less prominent than in the honey bee (Habenstein et al., 2023) or fruit fly (Ito et al., 2014), and it appears to be undivided, as in the cockroach (Althaus et al., 2022; Homberg et al., 2018). In contrast, the BU in the desert locust constitutes two spatially separated subunits, a medial and a lateral part (Hensgen, Göthe, et al., 2021; Träger et al., 2008). The BU houses arborizations of GABA-immunoreactive tangential neurons of the CBL and is part of the sky-compass pathway (*S. gregaria*: Homberg et al., 2023; *D. plexippus*: Beetz & el Jundi, 2023; Heinze & Reppert, 2011; *A. mellifera*: Held et al., 2016; *D. melanogaster*: Hardcastle et al., 2021).

The nearby GA is defined by the arborization area of CL columnar neurons of the CBL (Hensgen, Göthe, et al., 2021; Hensgen, England, et al., 2021; Jahn et al., 2023). Although little is known about the neuronal organization of the mantis CX, we identified a distinct area between the ULAL and LLAL as the GA based on its identical position in the locust, cockroach, fruit fly, and honey bee (Hensgen, England, et al., 2021; Ito et al., 2014; Jahn et al., 2023). Future investigations using single-cell tracer injections will be necessary to confirm the identity of this region as the GA.

4.3 | SNP and LH

The LH, along with the MB, is a higher order neuropil involved in processing olfactory information from the AL. The LH can be easily identified by GABA immunolabeling and synapsin immunolabeling, as well as by tracing the prominent mALT that projects into it. In the mantis, the LH lies at the same position as in the Madeira cockroach (Althaus et al., 2022) and desert locust (von Hadeln et al., 2018) and is dorsally encased by the SLP. However, unlike in the fruit fly (Ito et al., 2014), dung beetles (Immonen et al., 2017), or desert ants (Haben-

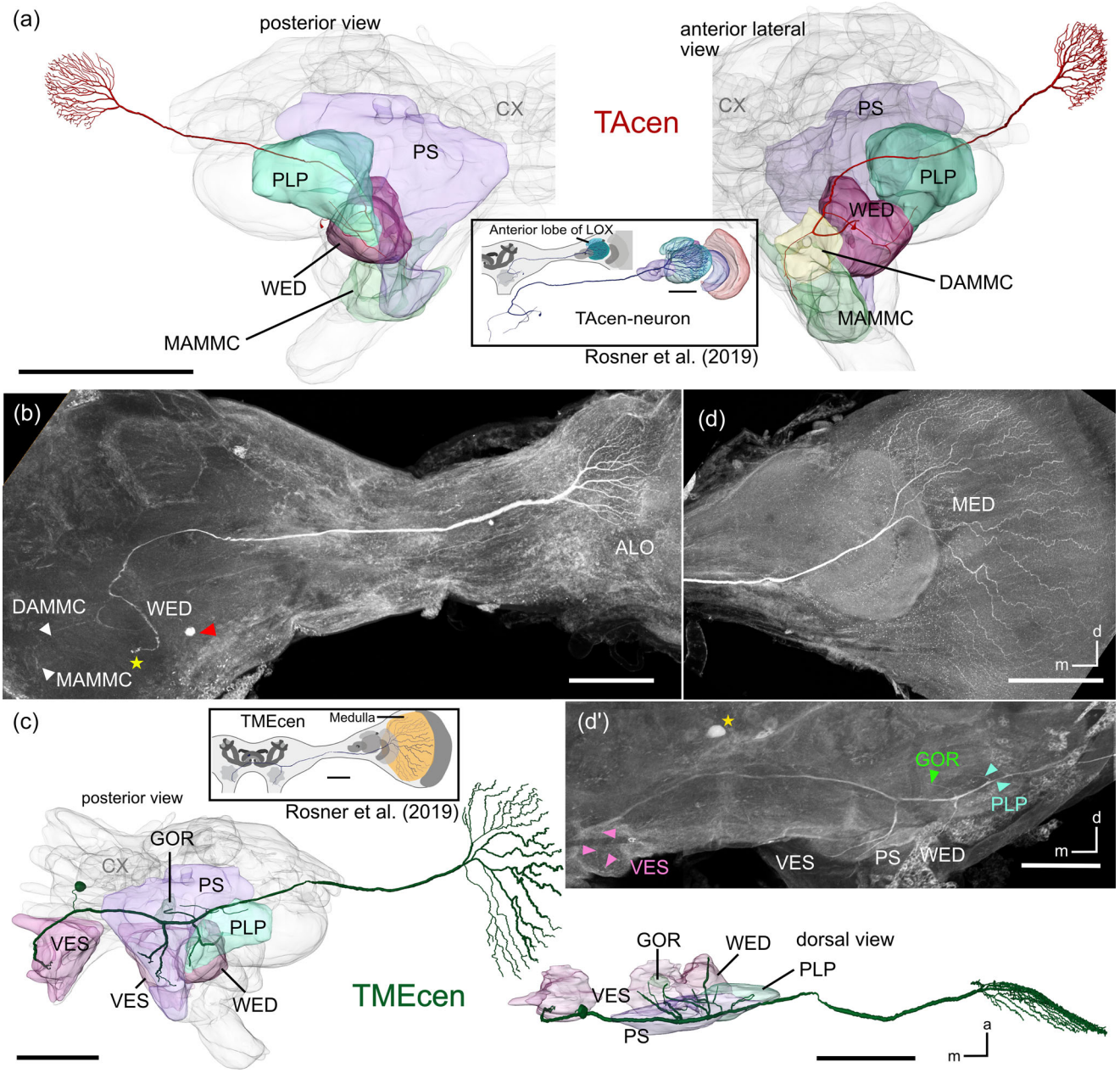

FIGURE 14 Three-dimensional reconstructions of the TAcen and the TMEcen neurons (Rosner et al., 2019). (a) Three-dimensional reconstruction of the TAcen neuron (Rosner et al., 2019) integrated into the half-transparent 3D atlas with innervated colored neuropils in anterior lateral (right) and posterior views (left). (b) Anterior projection view of the Neurobiotin-injected TAcen neuron, displaying 100 slices. Inset shows neuron from Rosner et al. (2019). Red arrowhead points to the soma, white arrowheads point to fine arborizations in the antennal mechanosensory and motor center (AMMC), and the yellow asterisk marks the connection to arborizations in the posterior brain. (c) Three-dimensional reconstruction of the TMEcen neuron integrated into the half-transparent 3D atlas with innervated neuropils in color, posterior (left) and dorsal (bottom right) views. Inset shows neuron from Rosner et al. (2019) in anterior view with innervated areas of the OL. (d) Anterior projection view of the TMEcen neuron from 60 slices showing the arborizations in the OL. (d') Anterior projection view of the Neurobiotin-injected TMEcen neuron from 115 slices of the central brain. Arrowheads point at neurites that are stained weakly. a, anterior; CX, central complex; d, dorsal; DAMMC, dorsal AMMC; GOR, gorget; m, medial; MAMMC, medial AMMC; PS, posterior slope; VES, vest; WED, wedge. Scale bars = 600 µm (a), 400 µm (b, c), and 200 µm (d, d').

stein et al., 2020), the LH in the mantis is not laterally attached to the SLP.

The SLP, SIP, and SMP, forming the dorsal face of the brain, are distinguished in all available insect brain atlases. These neuropils contain prominent arborization areas of neurosecretory cells of the pars intercerebralis and lateralis (Reinhard et al., 2022). In mantises, the SMP is relatively large and fused across the midline, similar to the SMP in dung beetles (Immonen et al., 2017), where it is directly attached to the midline crossing ATL. This is in contrast to other polyneopteran insects where the SMPs of both hemispheres are not fused and appear smaller

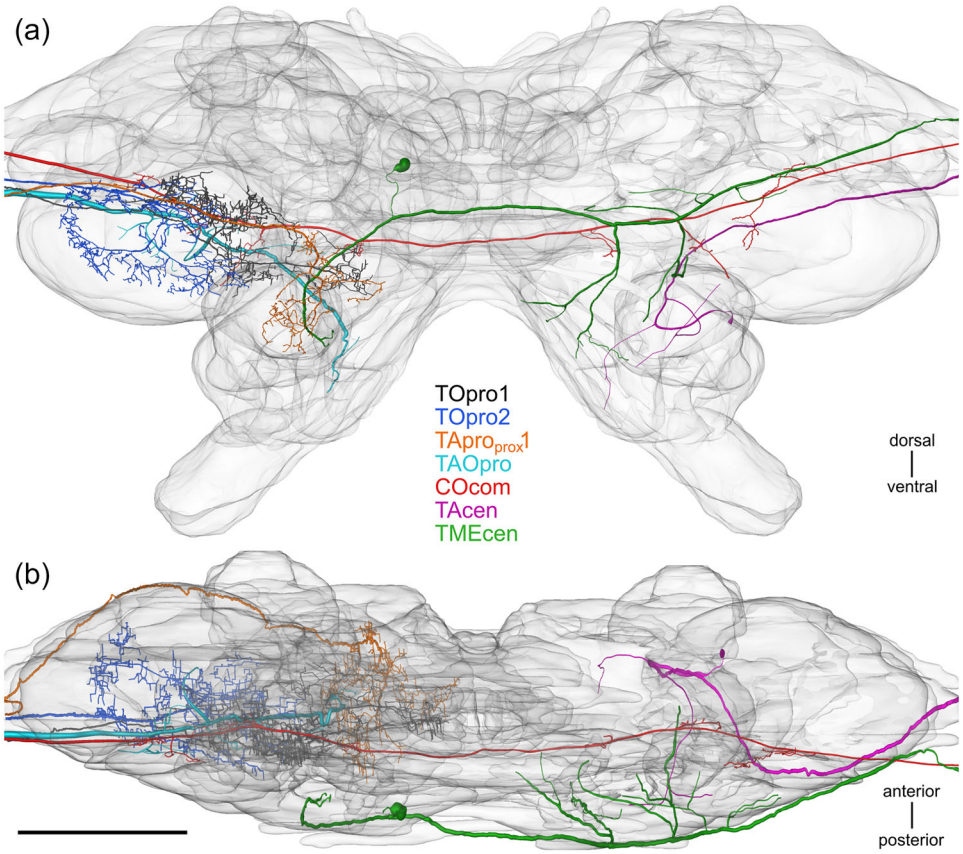

FIGURE 15 Integration of all seven reconstructed optic lobe neurons (Figures 11–14) into the semi-transparent 3D atlas of the mantis cerebrum. Frontal posterior view (a) and dorsal view (b) showing the spatial arrangement of branching areas in the brain. Scale bar = 300 µm.

(Althaus et al., 2022; von Hadeln et al., 2018). An additional distinct neuropil, the ABR, was identified within the SNP, which is apparently exclusive to polyneopteran insects. The ABR spans the midline and covers the anterodorsal part of the SMP. It could be clearly distinguished by its fibrous structure observed in synapsin immunolabeling. In other insects, it may have been considered as part of the SMP (Habenstein et al., 2020, 2023; Ito et al., 2014). The SIP, like the SMP and SLP, extends from the anterior to the posterior surface of the brain. Its position and shape strongly correspond to those in other polyneopteran insects, but it occupies more space than in the fruit fly (Ito et al., 2014). In the mantis, the SIP does not completely surround the VL, but rather covers its dorsal surface and surrounds it anteriorly. Tracing experiments conducted in fruit flies have revealed that olfactory information from the LH may enter the SLP and SCL, possibly forming connections to the SIP and SMP (Yu et al., 2013). In honey bees, the SIP (also known as the ring neuropil) is targeted by output neurons from the MB (Abel et al., 2001; Rybak & Menzel, 1993).

4.4 | Ventrolateral neuropils

The VLP in the mantis mirrors the shape and position observed in the cockroach and locust (Althaus et al., 2022; von Hadeln et al., 2018) and is divided into an anterior and posterior region in all three species. The PVLP has been described as a region with glomerular structure in flies and bumblebees (Ito et al., 2014; Paulk et al., 2009), and we have, likewise, identified a glomerular organization in the mantis brain (Figure 8h). In *D. melanogaster*, the WED and PVLP serve as secondary auditory neuropils connected by interneurons to auditory afferents from Johnston's organ that terminate in the AMMC (Matsuo et al., 2016; Patella & Wilson, 2018). Direct input from Johnston's organ to the VLP was also found in ants (Grob et al., 2021). In desert locusts, the PLP and PVLP receive massive input from ascending neurons providing auditory and cercal wind-sensory input (Staudacher et al., 2023). The glomerular organization of the PVLP and PLP in *D. melanogaster* is largely based on a visual feature map provided by parallel projections of lobula columnar neurons signaling various aspects of moving objects (Aptekar et al., 2015; Klapoetke et al., 2022; Wu et al., 2016). As shown in the fruit fly and silk moth, some of these sensory inputs likely converge onto specific descending neurons (Namiki, Dickinson, et al., 2018; Namiki, Wada, et al., 2018). In the mantis, the VLP and WED, likewise, receive prominent input from visual interneurons (Table 1). Consequently, the VLNP in the mantis might function as a premotor center, processing visual data and facilitating swift, accurate responses to visual stimuli.

The anterior ventrolateral area of the mantis brain houses the AOTU, which consists of a larger UU and a smaller LU separated by the TUBUT. The separation of the AOTU into UU and LU appears to be

consistent across various insect species, while the number of subunits of the LU appears to be more variable (Adden et al., 2020; Hardcastle et al., 2021; Heinze & Reppert, 2012; Homberg et al., 2003; Immonen et al., 2017; Mota et al., 2011). The LU of the AOTU is involved in the processing of celestial cues, including the sun's position and the polarization pattern of the sky (Hardcastle et al., 2021; Homberg et al., 2023), while the UU receives LOX input from neurons involved in object detection (Aptekar et al., 2015; Collett, 1972; Ribeiro et al., 2018). This information is transmitted through the TUBUT, via the BU, and a parallel fiber bundle via the LAL to the CX, where further processing related to goal-directed navigation takes place (Hardcastle et al., 2021; Heinze, 2017; Homberg et al., 2003, 2023). While central neural substrates such as the AOTU, TUBUT, and its connection to the CX are present in the mantis, their involvement in sky compass orientation or other functions still needs to be established.

4.5 | Inferior neuropils

The large group of INP includes the CRE. In the fruit fly, the CRE surrounds the shaft of the ML, which has not been observed in the mantis, locust (von Hadeln et al., 2018), and cockroach (Althaus et al., 2022). GABA-immunolabeled fibers from the CRE target the CA (Strausfeld & Li, 1999; Yamazaki et al., 1998) and have also served in the cockroach brain for the identification of the CRE (Althaus et al., 2022). In the fruit fly (Ito et al., 2014) and cockroach (Althaus et al., 2022), a small spherical neuropil is part of the CRE, called the rubus (RUB). While we were unable to distinguish the RUB by synapsin labeling in the mantis, it may be identified by tracer injections into columnar neurons of the CBU, whose arborizations outside the CX are confined to the RUB (Hulse et al., 2021; Ito et al., 2014; Jahn et al., 2023). The remaining parts of the CRE are connected to the LAL as examined in the locust (Hensgen, Göthe, et al., 2021) and fruit fly (Hulse et al., 2021). In the fruit fly, the CRE is also innervated by output neurons of the MB (Li et al., 2020), although little is known about the physiology of these neurons.

The SCL and ICL in the mantis stretch from the CB to the lateral SLP. In the fruit fly, the CL is divided into SLC and ILC by the superior arch- and ellipsoid commissures (Ito et al., 2014). Because we did not observe corresponding landmarks in the mantis, we referred to the 3D atlases of the locust (von Hadeln et al., 2018) and the cockroach brain (Althaus et al., 2022), where the CL was subdivided with the help of the arising PED. Medially adjacent to the ICL, the IB crosses the posterior brain midline. The IB has been identified in the brains of the locust, cockroach, dung beetle, ant, honey bee, and fly, but not in *Tribolium castaneum* (Farnworth et al., 2022), *C. obscurior* (Bressan et al., 2015), *A. infusa* (Adden et al., 2020), and *D. plexippus* (Heinze & Reppert, 2012). The IB in the mantis was, as in the locust and cockroach, discernible due to strong synapsin staining and the lateral adjoining fascicles (MEF and LEF).

The ATL in the mantis differs in its shape from that of other insect species. It is fused at the midline and elongated along the dorsal surface of the IB. This suggests that, similar to the findings in *D. melanogaster* (Ito et al., 2014), the ATL may be part of the IB. This is consistent with our results, as the ATL was difficult to differentiate from the IB and shows elongation along its dorsal surface. In contrast, the OR was much easier to identify by tracing the course of the OCN. In *H. membranacea*, the number of ocelli corresponds to the number of the ORs in the brain, with one ocellus per hemisphere. The ORs serve as the input station of visual input from the ocelli. Their position is similar to those in the locust (von Hadeln et al., 2018) and cockroach (Althaus et al., 2022). The mantis brain features a quite prominent MAL, which has not been described in holometabolous insects but is easily distinguishable in polyneopteran insects. In the mantis, the MAL is fused across the midline, as in the locust (von Hadeln et al., 2018), but different from the more closely related Madeira cockroach where it does not span the midline (Althaus et al., 2022).

4.6 | Ventromedial neuropils

The functional role of the VMNP is not well understood. The POTU is involved in the processing of celestial cues and is connected to the PB via tangential neurons. In the cockroach (*R. maderae*), the POTU is also associated with the circadian system and is strongly labeled by antisera against pigment-dispersing factor (Stengl & Homberg, 1994). In the mantis, we specified the POTU by TH labeling, along with the identification of the POC that projects to the POTU and connects both OLs. In *D. melanogaster*, the PS is subdivided into a superior and an inferior region separated by the POC (Ito et al., 2014). In the mantis, a subdivision, like in the cockroach, dung beetles, and locust (Althaus et al., 2022; Immonen et al., 2017; von Hadeln et al., 2018), was not obvious. The PS is a major target of motion-sensitive projection neurons from the ME and LOX signaling ego motion (Namiki, Dickinson, et al., 2018; Paulk et al., 2008, 2009; Ryu et al., 2022; Strausfeld, 1976; Strausfeld & Bassemir, 1985a, 1985b; Suver et al., 2016) and is innervated by numerous descending and ascending neurons (Okada et al., 2003; Ryu et al., 2022; Staudacher, 1998; Staudacher et al., 2023; Strausfeld, 1976). In addition, the PS receives input from numerous brain areas including the LAL, as reported in the silk moth (*Bombyx mori*), where these neurons seem to be involved in motor control for pheromone processing (Namiki, Wada, et al., 2018). Neurons connecting the LAL and PS in the desert locust may play a role in spatial orientation (Heinze & Homberg, 2009). As shown in Table 1, seven out of 15 characterized visual interneurons of the OL of the mantis arborize in the PS. Five out of these are projection neurons from the LOX that may target descending neurons in the PS for initiating orientation responses. The presence of branches within the LAL in one of these neurons (Table 1, TADpro) shows parallel processing of visual input in the PS and LAL.

The VX comprises the EPA, GOR, and VES, with the VES being the largest region. This organization aligns with findings from *D. melanogaster* (Ito et al., 2014), *S. gregaria* (von Hadeln et al., 2018), and *R. maderae* (Althaus et al., 2022). In the monarch butterfly, the VX is reconstructed as a single structure within the ventromedial anterior neuropil (Heinze & Reppert, 2012), while in ants, it is considered part of the ventromedial protocerebrum (Bressan et al., 2015). Major landmarks for identifying the VES in the mantis are the IFS and GC, as also reported in

other established brain atlases. The EPA and GOR are dorsally attached to the VES and have similar positions in the fruit fly (Ito et al., 2014). In the mantis, the GOR was difficult to distinguish and could only be identified by its shape and position, similar to data in the fruit fly (Ito et al., 2014) and in the cockroach (Althaus et al., 2022).

4.7 | PENP, TC, and the AL

Many insects rely on olfactory stimuli for various behaviors, such as foraging or searching for sexual partners. Despite the relatively small size of their antennae, studies have shown that praying mantises are responsive to olfactory cues (Allen et al., 2012; Carle et al., 2014). Male mantises can recognize a female's willingness to mate based on sex pheromones released by the females (Lelito & Brown, 2008). The primary olfactory center of insects is the glomerular AL (Hansson & Anton, 2000). In *H. membranacea*, the AL has relatively large glomeruli, similar to those in the cockroach (*R. maderae*), although in a smaller number, probably due to the mantis' strong reliance on visual input. In the Chinese mantis (*Tenodera aridifolia*), 54 glomeruli were identified in the AL (Carle et al., 2017), slightly less than the 61 glomeruli counted in *H. membranacea*. The glomeruli are connected through different AL tracts to higher brain areas for further processing of olfactory cues. We identified one of these tracts, the mALT, which contains a large number of projection neurons targeting the CA of the MB and LH.

The VFA is closely linked to the antennae and can be reliably identified by backfills of the antennal flagellum, as it receives massive innervation by flagellar afferents (Staudacher & Schildberger, 2000; Staudacher et al., 2005). In contrast, differentiating the mantis VFA solely by synapsin staining was difficult, unlike in the cockroach or locust, where the VFA is a synapsin-rich area between the AL and GLO (Althaus et al., 2022; von Hadeln et al., 2018). The mantis VFA is relatively small compared to the VFA of the cricket or cockroach, which may relate to differences in lifestyle and the less prominent organization of the mantis antennae. The VFA has not been recognized in holometabolous insects studied thus far. It is part of the AMMC, which also includes the DAMMC, LAMMC, and MAMMC. In fruit flies, these regions likely correspond to the saddle, which contains the fly AMMC. The organization of the mantis AMMC into a dorsal, medial, and lateral region follows the corresponding organization in the locust (von Hadeln et al., 2018). The subdivisions were established by considering their spatial arrangement in the brain and were aided by antennal backfills.

The GLO, a termination site for maxillary palp afferents in polyneopteran insects (Ignell et al., 2000), was also identified in a holometabolous insect, the beetle *T. castaneum* (Dippel et al., 2016). It was proposed that the GLO is involved in odor processing by olfactory neurons of the mouthparts, without involvement of the ALs (Dippel et al., 2016). In the migratory locust (*Locusta migratoria*), the GLO is involved in odor-induced vomiting (Sun et al., 2022). In the cockroach (*R. maderae*), the GLO is a highly glomerular neuropil and is easily identified using synapsin immunolabeling (Althaus et al., 2022). In the mantis, the GLO is less prominent and was only established by backfills of the maxillary palps. The GLO is assumed to be of tritocerebral origin, because the TC is, among other neuronal connections, innervated by nerves from the mouthparts and the stomatogastric system (Aubele & Klemm, 1977; Farris, 2008; Rajashekhar & Singh, 1994). The mantis TC, the most ventral area of the central brain, appears to be undivided as in other polyneopteran insects (Althaus et al., 2022; von Hadeln et al., 2018). Owing to fusion of the gnathal and cerebral ganglia in holometabolous insects, its correspondence with neuropils like the prow and saddle in the fruit fly (Ito et al., 2014) is difficult and has not been investigated.

4.8 | Insights from ramification sites of optic lobe neurons

We integrated seven neurons published previously (Rosner et al., 2019, 2020) into the mantis brain atlas (Figures 11–15) and, in addition, provide detailed information about ramification sites of additional neurons not integrated here (Table 1). Registration of neurons from different experiments into a reference system is usually done by warping different brains into an average standardized 3D brain atlas to be used as a common platform (el Jundi & Heinze, 2020; Rybak et al., 2010). However, integration of neurons from different brains into a 3D-reconstructed single brain, as done here, has previously also been achieved for the CX of the dung beetle (el Jundi et al., 2018). That study, based on transformation of neurons using 12 degrees of freedom, revealed detailed information on the layering and columnar organization of the CX. Integration of the mantis neurons into the 3D brain atlas, in contrast, was achieved by transformation with only seven degrees of freedom (translation, rotation, and isotropic scaling). The high level of accuracy we obtained is illustrated by the fact that axonal fibers of all neurons were correctly positioned in the same fiber tracts in the 3D atlas as in their brain of origin (TOpro1, TOpro2, TAOpro, and COcom in GC; TApro$_{prox}$1 in AOT; TAOpro within IFS), although fiber tracts were not considered in the integration process. For future studies on neural networks in the mantis brain, it might, nevertheless, be useful to establish a standard 3D brain platform, which might reveal even more precision, especially when analyzing details in projection sites and possible synaptic contacts.

Rosner et al. (2017, 2019, 2020) suggested corresponding substructures in the LOX in mantises and flies. The data presented here support these claims. The fly LOX comprises two nested neuropils, the lobula plate and the lobula. Widefield motion is processed in a directionally selective manner in the lobula plate, while in the lobula, several types of projection neurons respond to motion of small, dark targets (Klapoetke et al., 2022; Ryu et al., 2022). In the mantis, widefield motion is processed in a directionally selective manner by neurons ramifying in distal layers of the ALO (TADpro, TApro$_{dist}$1, and TAcen in Rosner et al. [2019, 2020]; TAproM1 and TAproM2 in Yamawaki [2019]) and, additionally, by neurons with input exclusively in the dorsal lobe of the LOX (Yamawaki, 2019). Thus, these neurons share physiological properties with lobula plate tangential cells in flies. Lobula plate tangential cells have central brain ramifications in the PS and PLP but not in the VLP

(Ito et al., 2014; Namiki, Wada, et al., 2018; Ryu et al., 2022). As shown here, this also holds for the investigated widefield sensitive cells in the mantis (TADpro, TAPro$_{dist}$1, and TAcen).

All other LOX neurons presented in Table 1 ramify in the VLP (AVLP or PVLP). In the fly, VLP ramifications are indicative of lobula neurons (Ito et al., 2014; Otsuna & Ito, 2006). Mantis neurons that have LOX ramifications exclusively in the OLO or the SLO (TOproM/TOpro1, TOproL, COcom, and Scom) respond strongly to motion of small, dark, prey-like objects (Rosner et al., 2020; Yamawaki, 2019). The physiological features of the OLO and SLO in conjunction with the VLP ramifications of neurons originating in OLO and SLO (TOpro1, TOpro2, COcom, TOpro3, and Spro in Table 1) support previous claims that the OLO, perhaps together with the SLO, corresponds to the fly lobula.

Two tangential projection neurons (TAPro$_{prox}$1 and TADpro) provide input to the LAL. TAPro$_{prox}$1 responds to dark flashing bars (Rosner et al., 2020), while the TADpro/TAproM2 neuron responds best to bright flashing bars and moving gratings, that is, widefield motion (Rosner et al., 2020; Yamawaki, 2019). The LALs are sensory motor relay neuropils that are highly linked with the CX. In bees, the CX is suspected to harbor neurons that determine traveled distances by integrating optic flow (Stone et al., 2017). Widefield motion-sensitive neurons in the CX suggested to play a role in distance perception receive input in the LALs (Stone et al., 2017). Thus, homologs of the mantis TADpro neuron in bees could link the optic lobe with the CX and provide signals for travel distance estimation in path integration.

The praying mantis is a formidable predator of the insect world with a highly specialized visual system attuned to detecting and hunting prey. The identification and 3D mapping of neuropils and fiber tracts in the mantis brain is an important step toward linking behavioral data to activities in particular brain areas. The mantis brain atlas has been enriched by integrating specific neurons previously studied, offering a more detailed understanding of the brain's structure and function. The data underscore potential homologies between the mantis and other insects, particularly in the LOX region. Distinct pathways in the LOX allow the mantis to detect both small moving objects and widefield motion, a feature also observed in flies. The integration of these neurons into the atlas not only provides insights into the unique visual system of the mantis, but also emphasizes the atlas as a tool for analyzing neural networks involved in visual perception and behavior.

AUTHOR CONTRIBUTIONS

Study concept and design: Ronny Rosner and Uwe Homberg. *Acquisition of data*: Ronny Rosner, Joss von Hadeln, Gesa Exner, and Vanessa Althaus. *Data analysis and interpretation*: Vanessa Althaus, Gesa Exner, Ronny Rosner, Joss von Hadeln, and Uwe Homberg. *Drafting of the manuscript*: Vanessa Althaus and Gesa Exner. *Review and editing*: Uwe Homberg, Ronny Rosner, and Vanessa Althaus.

ACKNOWLEDGMENTS

We are grateful to Drs. Erich Buchner and Christian Wegener (University of Würzburg) for donating antibodies against synapsin (SYNORF1) and to Dr. Timothy G. Kingan (University of Arizona) for donating the antiserum against GABA. We thank Martina Kern for performing the backfills of Figure 10, Stefanie Jahn for creating the supplemental movie, Josephine Timm for providing the immunolabeling of tyrosine hydroxylase of Figure 9h, Jutta Seyfarth for performing the GABA immunolabeling of the mantis brain, and Dr. Erich Staudacher for his time and expertise in interpreting the backfill data.

Open access funding enabled and organized by Projekt DEAL.

CONFLICT OF INTEREST STATEMENT

The authors declare no conflicts of interest.

DATA AVAILABILITY STATEMENT

All data that support the findings of this study are available from the corresponding authors. The original full confocal gray-value data sets with neuropil demarcations are provided on Figshare (https://doi.org/10.6084/m9.figshare.25074674).

ORCID

Vanessa Althaus https://orcid.org/0000-0001-8018-0555
Uwe Homberg https://orcid.org/0000-0002-8229-7236
Ronny Rosner https://orcid.org/0000-0002-5829-8626

4.9 | PEER REVIEW

The peer review history for this article is available at https://publons.com/publon/10.1002/cne.25607

REFERENCES

Abel, R., Rybak, J., & Menzel, R. (2001). Structure and response patterns of olfactory interneurons in the honeybee, *Apis mellifera*. *Journal of Comparative Neurology*, *437*, 363–383. https://doi.org/10.1002/cne.1289

Adden, A., Wibrand, S., Pfeiffer, K., Warrant, E., & Heinze, S. (2020). The brain of a nocturnal migratory insect, the Australian Bogong moth. *Journal of Comparative Neurology*, *528*, 1942–1963. https://doi.org/10.1002/cne.24866

Allen, L. E., Barry, K. L., & Holwell, G. I. (2012). Mate location and antennal morphology in the praying mantid *Hierodula majuscula*. *Australian Journal of Entomology*, *51*, 133–140. https://doi.org/10.1111/j.1440-6055.2011.00843.x

Althaus, V., Jahn, S., Massah, A., Stengl, M., & Homberg, U. (2022). 3D-atlas of the brain of the cockroach *Rhyparobia maderae*. *Journal of Comparative Neurology*, *530*, 3126–3156. https://doi.org/10.1002/cne.25396

Aptekar, J. W., Keleş, M. F., Lu, P. M., Zolotova, N. M., & Frye, M. A. (2015). Neurons forming optic glomeruli compute figure–ground discriminations in *Drosophila*. *Journal of Neuroscience*, *35*, 7587–7599. https://doi.org/10.1523/JNEUROSCI.0652-15.2015

Aubele, E., & Klemm, N. (1977). Origin, destination and mapping of tritocerebral neurons of locust. *Cell and Tissue Research*, *178*, 199–219. https://doi.org/10.1007/BF00219048

Avarguès-Weber, A., Deisig, N., & Giurfa, M. (2011). Visual cognition in social insects. *Annual Review of Entomology*, *56*, 423–443. https://doi.org/10.1146/annurev-ento-120709-144855

Beetz, M. J., & el Jundi, B. (2023). The neurobiology of the Monarch butterfly compass. *Current Opinion in Insect Science*, *60*, 101109. https://doi.org/10.1016/j.cois.2023.101109

Brandt, R., Rohlfing, T., Rybak, J., Krofczik, S., Maye, A., Westerhoff, M., Hege, H.-C., & Menzel, R. (2005). Three-dimensional average-shape atlas of the honeybee brain and its applications. *Journal of Comparative Neurology*, *492*, 1–19. https://doi.org/10.1002/cne.20644

Bressan, J. M. A., Benz, M., Oettler, J., Heinze, J., Hartenstein, V., & Sprecher, S. G. (2015). A map of brain neuropils and fiber systems in the ant *Cardiocondyla obscurior*. *Frontiers in Neuroanatomy*, *8*, 166. https://doi.org/10.3389/fnana.2014.00166

Calvo, A. C., Pey, A. L., Miranda-Vizuete, A., Døskeland, A. P., & Martinez, A. (2011). Divergence in enzyme regulation between *Caenorhabditis elegans* and human tyrosine hydroxylase, the key enzyme in the synthesis of dopamine. *Biochemical Journal*, *434*, 133–141. https://doi.org/10.1042/BJ20101561

Carle, T., Toh, Y., Yamawaki, Y., Watanabe, H., & Yokohari, F. (2014). The antennal sensilla of the praying mantis *Tenodera aridifolia*: A new flagellar partition based on the antennal macro-, micro- and ultrastructures. *Arthropod Structure & Development*, *43*, 103–116. https://doi.org/10.1016/j.asd.2013.10.005

Carle, T., Watanabe, H., Yamawaki, Y., & Yokohari, F. (2017). Organization of the antennal lobes in the praying mantis (*Tenodera aridifolia*). *Journal of Comparative Neurology*, *525*, 1685–1706. https://doi.org/10.1002/cne.24159

Chiang, A. S., Lin, C. Y., Chuang, C. C., Chang, H. M., Hsieh, C. H., Yeh, C. W., Shih, C. T., Wu, J. J., Wang, G. T., Chen, Y. C., Wu, C. C., Chen, G. Y., Ching, Y. T., Lee, P. C., Lin, C. Y., Lin, H. H., Wu, C. C., Hsu, H. W., Huang, Y. A., … Hwang, J. K. (2011). Three-dimensional reconstruction of brain-wide wiring networks in *Drosophila* at single-cell resolution. *Current Biology*, *21*, 1–11. https://doi.org/10.1016/j.cub.2010.11.056

Collett, T. (1972). Visual neurones in the anterior optic tract of the privet hawk moth. *Journal of Comparative Physiology*, *78*, 396–433. https://doi.org/10.1007/BF01417943

Dippel, S., Kollmann, M., Oberhofer, G., Montino, A., Knoll, C., Krala, M., Rexer, K.-H., Frank, S., Kumpf, R., Schachtner, J., & Wimmer, E. A. (2016). Morphological and transcriptomic analysis of a beetle chemosensory system reveals a gnathal olfactory center. *BMC Biology*, *14*, 90. https://doi.org/10.1186/s12915-016-0304-z

el Jundi, B., Heinze, S., Lenschow, C., Kurylas, A., Rohlfing, T., & Homberg, U. (2010). The locust standard brain: A 3D standard of the central complex as a platform for neural network analysis. *Frontiers in Systems Neuroscience*, *3*, 21. https://doi.org/10.3389/neuro.06.021.2009

el Jundi, B., & Heinze, S. (2020). Three-dimensional atlases of insect brains. In R. Pelc, W. Walz, & J. R. Doucette (Eds.), *Neurohistology and imaging techniques. Neuromethods* (Vol. 153, pp. 73–124). Humana. https://doi.org/10.1007/978-1-0716-0428-1_3

el Jundi, B., Warrant, E. J., Pfeiffer, K., & Dacke, M. (2018). Neuroarchitecture of the dung beetle central complex. *Journal of Comparative Neurology*, *526*, 2612–2630. https://doi.org/10.1002/cne.24520

Fahrbach, S. E. (2006). Structure of the mushroom bodies of the insect brain. *Annual Review of Entomology*, *51*, 209–232. https://doi.org/10.1146/annurev.ento.51.110104.150954

Farnworth, M. S., Bucher, G., & Hartenstein, V. (2022). An atlas of the developing *Tribolium castaneum* brain reveals conservation in anatomy and divergence in timing to *Drosophila melanogaster*. *Journal of Comparative Neurology*, *530*, 2335–2371. https://doi.org/10.1002/cne.25335

Farris, S. M. (2008). Tritocerebral tract input to the insect mushroom bodies. *Arthropod Structure & Development*, *37*, 492–503. https://doi.org/10.1016/j.asd.2008.05.005

Giurfa, M. (2021). Learning of sameness/difference relationships by honey bees: Performance, strategies and ecological context. *Current Opinion in Behavioral Sciences*, *37*, 1–6. https://doi.org/10.1016/j.cobeha.2020.05.008

Gonzalez-Bellido, P. T., Fabian, S. T., & Nordström, K. (2016). Target detection in insects: Optical, neural and behavioral optimizations. *Current Opinion in Neurobiology*, *41*, 122–128. https://doi.org/10.1016/j.conb.2016.09.001

Grob, R., Tritscher, C., Grübel, K., Stigloher, C., Groh, C., Fleischmann, P. N., & Rössler, W. (2021). Johnston's organ and its central projections in *Cataglyphis* desert ants. *Journal of Comparative Neurology*, *529*, 2138–2155. https://doi.org/10.1002/cne.25077

Habenstein, J., Amini, E., Grübel, K., el Jundi, B., & Rössler, W. (2020). The brain of *Cataglyphis* ants: Neuronal organization and visual projections. *Journal of Comparative Neurology*, *528*, 3479–3506. https://doi.org/10.1002/cne.24934

Habenstein, J., Grübel, K., Pfeiffer, K., & Rössler, W. (2023). 3D atlas of cerebral neuropils with previously unknown demarcations in the honey bee brain. *Journal of Comparative Neurology*, *531*, 1163–1183. https://doi.org/10.1002/cne.25486

Hamanaka, Y., Minoura, R., Nishino, H., Miura, T., & Mizunami, M. (2016). Dopamine- and tyrosine hydroxylase-immunoreactive neurons in the brain of the American cockroach, *Periplaneta americana*. *PLoS ONE*, *11*, e0160531. https://doi.org/10.1371/journal.pone.0160531

Hansson, B. S., & Anton, S. (2000). Function and morphology of the antennal lobe: New developments. *Annual Review of Entomology*, *45*, 203–231. https://doi.org/10.1146/annurev.ento.45.1.203

Hardcastle, B. J., Omoto, J. J., Kandimalla, P., Nguyen, B.-C. M., Keleş, M. F., Boyd, N. K., Hartenstein, V., & Frye, M. A. (2021). A visual pathway for skylight polarization processing in *Drosophila*. *eLife*, *10*, e63225. https://doi.org/10.7554/eLife.63225

Heinze, S. (2017). Unraveling the neural basis of insect navigation. *Current Opinion in Insect Science*, *24*, 58–67. https://doi.org/10.1016/j.cois.2017.09.001

Heinze, S., & Homberg, U. (2008). Neuroarchitecture of the central complex of the desert locust: Intrinsic and columnar neurons. *Journal of Comparative Neurology*, *511*, 454–478. https://doi.org/10.1002/cne.21842

Heinze, S., & Homberg, U. (2009). Linking the input to the output: New sets of neurons complement the polarization vision network in the locust central complex. *Journal of Neuroscience*, *29*, 4911–4921. https://doi.org/10.1523/JNEUROSCI.0332-09.2009

Heinze, S., Narendra, A., & Cheung, A. (2018). Principles of insect path integration. *Current Biology*, *28*, R1043–R1058. https://doi.org/10.1016/j.cub.2018.04.058

Heinze, S., & Reppert, S. M. (2011). Sun compass integration of skylight cues in migratory monarch butterflies. *Neuron*, *69*, 345–358. https://doi.org/10.1016/j.neuron.2010.12.025

Heinze, S., & Reppert, S. M. (2012). Anatomical basis of sun compass navigation I: The general layout of the monarch butterfly brain. *Journal of Comparative Neurology*, *520*, 1599–1628. https://doi.org/10.1002/cne.23054

Heinze, S., Florman, J., Asokaraj, S., el Jundi, B., & Reppert, S. M. (2013). Anatomical basis of sun compass navigation II: The neuronal composition of the central complex of the monarch butterfly. *Journal of Comparative Neurology*, *521*, 267–298. https://doi.org/10.1002/cne.23214

Heisenberg, M. (1998). What do the mushroom bodies do for the insect brain? An introduction. *Learning & Memory*, *5*, 1–10. https://doi.org/10.1101/lm.5.1.1

Held, M., Berz, A., Hensgen, R., Muenz, T. S., Scholl, C., Rössler, W., Homberg, U., & Pfeiffer, K. (2016). Microglomerular synaptic complexes in the sky-compass network of the honeybee connect parallel pathways from the anterior optic tubercle to the central complex. *Frontiers in Behavioral Neuroscience*, *10*, 186. https://doi.org/10.3389/fnbeh.2016.00186

Hensgen, R., Göthe, J., Jahn, S., Hümmert, S., Schneider, K. L., Takahashi, N., Pegel, U., Gotthardt, S., & Homberg, U. (2021). Organization and neural connections of the lateral complex in the brain of the desert locust. *Journal of Comparative Neurology*, *529*, 3533–3560. https://doi.org/10.1002/cne.25209

Hensgen, R., England, L., Homberg, U., & Pfeiffer, K. (2021). Neuroarchitecture of the central complex in the brain of the honeybee: Neuronal cell types. *Journal of Comparative Neurology*, *529*(1), 159–186. https://doi.org/10.1002/cne.24941

Homberg, U., Hensgen, R., Jahn, S., Pegel, U., Takahashi, N., Zittrell, F., & Pfeiffer, K. (2023). The sky compass network in the brain of the desert locust. *Journal of Comparative Physiology A: Neuroethology, Sensory, Neural, and Behavioral Physiology*, *209*, 641–662. https://doi.org/10.1007/s00359-022-01601-x

Homberg, U., Hofer, S., Pfeiffer, K., & Gebhardt, S. (2003). Organization and neural connections of the anterior optic tubercle in the brain of the desert locust. *Journal of Comparative Neurology*, *462*, 415–430. https://doi.org/10.1002/cne.10771

Homberg, U., Humberg, T.-H., Seyfarth, J., Bode, K., & Quintero Pérez, M. (2018). GABA immunostaining in the central complex of dicondylian insects. *Journal of Comparative Neurology*, *526*, 2301–2318. https://doi.org/10.1002/cne.24497

Honkanen, A., Adden, A., da Silvas Freitas, J., & Heinze, S. (2019). The insect central complex and the neural basis of navigational strategies. *Journal of Experimental Biology*, *222*, (Pt Suppl 1), jeb188854. https://doi.org/10.1242/jeb.188854

Hoskins, S. G., Homberg, U., Kingan, T. G., Christensen, T. A., & Hildebrand, J. G. (1986). Immunocytochemistry of GABA in the antennal lobes of the sphinx moth *Manduca sexta*. *Cell and Tissue Research*, *244*, 243–252. https://doi.org/10.1007/BF00219199

Hulse, B. K., Haberkern, H., Franconville, R., Turner-Evans, D. B., Takemura, S. Y., Wolff, T., Noorman, M., Dreher, M., Dan, C., Parekh, R., Hermundstad, A. M., Rubin, G. M., & Jayaraman, V. (2021). A connectome of the *Drosophila* central complex reveals network motifs suitable for flexible navigation and context-dependent action selection. *eLife*, *10*, e66039. https://doi.org/10.7554/eLife.66039

Hurd, L. E. (1999) Ecology of praying mantises. In F. R. Prete, H. Wells, P. H. Wells, & L. E. Hurd (Eds.), *The praying mantids* (pp. 43–60). John Hopkins University Press.

Ignell, R., Anton, S., & Hansson, B. S. (2000). The maxillary palp sensory pathway of Orthoptera. *Arthropod Structure & Development*, *29*, 295–305. https://doi.org/10.1016/S1467-8039(01)00016-0

Immonen, E. V., Dacke, M., Heinze, S., & el Jundi, B. (2017). Anatomical organization of the brain of a diurnal and a nocturnal dung beetle. *Journal of Comparative Neurology*, *525*, 1879–1908. https://doi.org/10.1002/cne.24169

Ito, K., Shinomiya, K., Ito, M., Armstrong, J. D., Boyan, G., Hartenstein, V., Harzsch, S., Heisenberg, M., Homberg, U., Jenett, A., Keshishian, H., Restifo, L. L., Rössler, W., Simpson, J. H., Strausfeld, N. J., Strauss, R., & Vosshall, L. B. (2014). A systematic nomenclature for the insect brain. *Neuron*, *81*, 755–765. https://doi.org/10.1016/j.neuron.2013.12.017

Jahn, S., Althaus, V., Heckmann, J., Janning, M., Seip, A.-K., Takahashi, N., Grigoriev, C., Kolano, J., & Homberg, U. (2023). Neuroarchitecture of the central complex in the Madeira cockroach *Rhyparobia maderae*: Pontine and columnar neuronal cell types. *Journal of Comparative Neurology*, *531*, 1689–1714. https://doi.org/10.1002/cne.25535

Kaiser, A., Hensgen, R., Tschirner, K., Beetz, E., Wüstenberg, H., Pfaff, M., Mota, T., & Pfeiffer, K. (2022). A three-dimensional atlas of the honeybee central complex, associated neuropils and peptidergic layers of the central body. *Journal of Comparative Neurology*, *530*, 2416–2438. https://doi.org/10.1002/cne.25339

Kinoshita, M., & Homberg, U. (2017). Insect brains: Minute structures controlling complex behaviors. In S. Shigeno, Y. Murakami, & T. Nomura (Eds.), *Brain evolution by design. Diversity and commonality in animals* (pp. 123–151). Springer. https://doi.org/10.1007/978-4-431-56469-0_6

Klagges, B. R. E., Heimbeck, G., Godenschwege, T. A., Hofbauer, A., Pflugfelder, G. O., Reifegerste, R., Reisch, D., Schaupp, M., Buchner, S., & Buchner, E. (1996). Invertebrate synapsins: A single gene codes for several isoforms in *Drosophila*. *Journal of Neuroscience*, *16*, 3154–3165. https://doi.org/10.1523/JNEUROSCI.16-10-03154.1996

Klapoetke, N. C., Nern, A., Rogers, E. M., Rubin, G. M., Reiser, M. B., & Card, G. M. (2022). A functionally ordered visual feature map in the *Drosophila* brain. *Neuron*, *110*, 1700–1711. https://doi.org/10.1016/j.neuron.2022.02.013

Kral, K., & Prete, F. R. (1999). In the mind of a hunter: The visual world of the praying mantis. In F. R. Prete (Ed.), *Complex worlds from simpler nervous systems* (pp. 75–116). MIT Press.

Kurylas, A. E., Rohlfing, T., Krofczik, S., Jenett, A., & Homberg, U. (2008). Standardized atlas of the brain of the desert locust, *Schistocerca gregaria*. *Cell and Tissue Research*, *333*, 125–145. https://doi.org/10.1007/s00441-008-0620-x

Kvello, P., Løfaldli, B. B., Rybak, J., Menzel, R., & Mustaparta, H. (2009). Digital, three-dimensional average shaped atlas of the *Heliothis virescens* brain with integrated gustatory and olfactory neurons. *Frontiers in Systems Neuroscience*, *3*, 14. https://doi.org/10.3389/neuro.06.014.2009

Lelito, J. P., & Brown, W. D. (2008). Mate attraction by females in a sexually cannibalistic praying mantis. *Behavioral Ecology and Sociobiology*, *63*, 313–320. https://doi.org/10.1007/s00265-008-0663-8

Li, F., Lindsey, J. W., Marin, E. C., Otto, N., Dreher, M., Dempsey, G., Stark, I., Bates, A. S., Pleijzier, M. W., Schlegel, P., Nern, A., Takemura, S., Eckstein, N., Yang, T., Francis, A., Braun, A., Parekh, R., Costa, M., Scheffer, L. K., … Rubin, G. M. (2020). The connectome of the adult *Drosophila* mushroom body provides insights into function. *eLife*, *9*, e62576. https://doi.org/10.7554/eLife.62576

Matsuo, E., Seki, H., Asai, T., Morimoto, T., Miyakawa, H., Ito, K., & Kamikouchi, A. (2016). Organization of projection neurons and local neurons of the primary auditory center in the fruit fly *Drosophila melanogaster*. *Journal of Comparative Neurology*, *524*, 1099–1164. https://doi.org/10.1002/cne.23955

Menzel, R. (2022). In search for the retrievable memory trace in an insect brain. *Frontiers in Systems Neuroscience*, *16*, 876376. https://doi.org/10.3389/fnsys.2022.876376

Merlin, C., Heinze, S., & Reppert, S. M. (2012). Unraveling navigational strategies in migratory insects. *Current Opinion in Neurobiology*, *22*, 353–361. https://doi.org/10.1016/j.conb.2011.11.009

Modi, M. N., Shuai, Y., & Turner, G. C. (2020). The *Drosophila* mushroom body: From architecture to algorithm in a learning circuit. *Annual Review of Neuroscience*, *43*, 465–484. https://doi.org/10.1146/annurev-neuro-080317-0621333

Mota, T., Yamagata, N., Giurfa, M., Gronenberg, W., & Sandoz, J. C. (2011). Neural organization and visual processing in the anterior optic tubercle of the honey bee brain. *Journal of Neuroscience*, *31*, 11443–11456. https://doi.org/10.1523/JNEUROSCI.0995-11.2011

Mizunami, M., Weibrecht, J. M., & Strausfeld, N. J. (1998). Mushroom bodies of the cockroach: Their participation in place memory. *Journal of Comparative Neurology*, *402*, 520–537. https://doi.org/10.1002/(SICI)1096-9861(19981228)402:4%3C520::AID-CNE6%3E3.0.CO;2-K

Namiki, S., Dickinson, M. H., Wong, A. M., Korff, W., & Card, G. M. (2018). The functional organization of descending sensory-motor pathways in *Drosophila*. *eLife*, *7*, e34272. https://doi.org/10.7554/eLife.34272

Namiki, S., Wada, S., & Kanzaki, R. (2018). Descending neurons from the lateral accessory lobe and posterior slope in the brain of the silkmoth *Bombyx mori*. *Scientific Report*, *8*, 9663. https://doi.org/10.1038/s41598-018-27954-5

Nishino, H., Iwasaki, M., Yasuyama, K., Hongo, H., Watanabe, H., & Mizunami, M. (2012). Visual and olfactory input segregation in the mushroom body calyces in a basal neopteran, the American cockroach. *Arthropod Structure & Development*, *41*, 3–16. https://doi.org/10.1016/j.asd.2011.08.005

Nityananda, V., Bissianna, G., Tarawneh, G., & Read, J. (2016). Small or far away? Size and distance perception in the praying mantis. *Philosophical Transactions of the Royal Society of London. B, Biological Sciences*, *371*, 20150262. https://doi.org/10.1098/rstb.2015.0262

Nityananda, V., Joubier, C., Tan, J., Tarawneh, G., & Read, J. C. (2019). Motion-in-depth perception and prey capture in the praying mantis *Sphodromantis lineola*. *Journal of Experimental Biology*, *222*, jeb198614. https://doi.org/10.1242/jeb.198614

Nityananda, V., O'Keeffe, J., Umeton, D., Simmons, A., & Read, J. C. (2019). Second-order cues to figure motion enable object detection during prey capture by praying mantises. *Proceedings of the National Academy of Sciences of the United States of America*, *116*, 27018–27027. https://doi.org/10.1073/pnas.19123101

Nityananda, V., Tarawneh, G., Rosner, R., Nicolas, J., Crichton, S., & Read, J. (2016). Insect stereopsis demonstrated using a 3D insect

cinema. *Scientific Report*, *6*, 18718. https://doi.org/10.1038/srep18718

Nordström, K., & O'Carroll, D. C. (2009). Feature detection and the hypercomplex property in insects. *Trends in Neurosciences*, *32*, 383–391. https://doi.org/10.1016/j.tins.2009.03.004

O'Carroll, D. (1993). Feature-detecting neurons in dragonflies. *Nature*, *362*, 541–543. https://doi.org/10.1038/362541a0

Okada, R., Sakura, M., & Mizunami, M. (2003). Distribution of dendrites of descending neurons and its implications for the basic organization of the cockroach brain. *Journal of Comparative Neurology*, *458*, 158–174. https://doi.org/10.1002/cne.10580

Olberg, R. M. (2012). Visual control of prey-capture flight in dragonflies. *Current Opinion in Neurobiology*, *22*, 267–271. https://doi.org/10.1016/j.conb.2011.11.015

Otsuna, H., & Ito, K. (2006). Systematic analysis of the visual projection neurons of *Drosophila melanogaster*. I. Lobula-specific pathways. *Journal of Comparative Neurology*, *497*, 928–958. https://doi.org/10.1002/cne.21015

Patella, P., & Wilson, R. I. (2018). Functional maps of mechanosensory features in the *Drosophila* brain. *Current Biology*, *28*, 1189–1203. https://doi.org/10.1016/j.cub.2018.02.074

Paulk, A. C., Phillips-Portillo, J., Dacks, A. M., Fellous, J. M., & Gronenberg, W. (2008). The processing of color, motion, and stimulus timing are anatomically segregated in the bumblebee brain. *Journal of Neuroscience*, *28*, 6319–6332. https://doi.org/10.1523/JNEUROSCI.1196-08.2008

Paulk, A. C., Dacks, A. M., Phillips-Portillo, J., Fellous, J. M., & Gronenberg, W. (2009). Visual processing in the central bee brain. *Journal of Neuroscience*, *29*, 9987–9999. https://doi.org/10.1523/JNEUROSCI.1325-09.2009

Pfeiffer, K. (2022). The neuronal building blocks of the navigational toolkit in the central complex of insects. *Current Opinion in Insect Science*, *55*, 100972. https://doi.org/10.1016/j.cois.2022.100972

Pfeiffer, K., & Homberg, U. (2014). Organization and functional roles of the central complex in the insect brain. *Annual Review of Entomology*, *59*, 165–184. https://doi.org/10.1146/annurev-ento-011613-162031

Poteser, M., & Kral, K. (1995). Visual distance discrimination between stationary targets in praying mantis: An index of the use of motion parallax. *Journal of Experimental Biology*, *198*, 2127–2137. https://doi.org/10.1242/jeb.198.10.2127

Rajashekhar, K. P., & Singh, R. N. (1994). Neuroarchitecture of the tritocerebrum of *Drosophila melanogaster*. *Journal of Comparative Neurology*, *349*, 633–645. https://doi.org/10.1002/cne.903490410

Read, J. C. (2023). Stereopsis without correspondence. *Philosophical Transactions of the Royal Society B: Biological Sciences*, *378*, 20210449. https://doi.org/10.1098/rstb.2021.0449

Reinhard, N., Schubert, F. K., Bertolini, E., Hagedorn, N., Manoli, G., Sekiguchi, M., Yoshii, T., Rieger, D., & Helfrich-Förster, C. (2022). The neuronal circuit of the dorsal circadian clock neurons in *Drosophila melanogaster*. *Frontiers in Physiology*, *13*, 886432. https://doi.org/10.3389/fphys.2022.886432

Ribeiro, I. M., Drews, M., Bahl, A., Machacek, C., Borst, A., & Dickson, B. J. (2018). Visual projection neurons mediating directed courtship in *Drosophila*. *Cell*, *174*, 607–621. https://doi.org/10.1016/j.cell.2018.06.020

Rosner, R., Tarawneh, G., Lukyanova, V., & Read, J. C. (2020). Binocular responsiveness of projection neurons of the praying mantis optic lobe in the frontal visual field. *Journal of Comparative Physiology A: Neuroethology, Sensory, Neural, and Behavioral Physiology*, *206*, 165–181. https://doi.org/10.1007/s00359-020-01405-x

Rosner, R., von Hadeln, J., Salden, T., & Homberg, U. (2017). Anatomy of the lobula complex in the brain of the praying mantis compared to the lobula complexes of the locust and cockroach. *Journal of Comparative Neurology*, *525*, 2343–2357. https://doi.org/10.1002/cne.24208

Rosner, R., von Hadeln, J., Tarawneh, G., & Read, J. C. (2019). A neuronal correlate of insect stereopsis. *Nature Communications*, *10*, 2845. https://doi.org/10.1038/s41467-019-10721-z

Rossel, S. (1979). Regional differences in photoreceptor performance in the eye of the praying mantis. *Journal of Comparative Physiology*, *131*, 95–112. https://doi.org/10.1007/BF00619070

Rossel, S. (1983). Binocular stereopsis in an insect. *Nature*, *302*, 821–822. https://doi.org/10.1038/302821a0

Ryu, L., Kim, S. Y., & Kim, A. J. (2022). From photons to behaviors: Neural implementations of visual behaviors in *Drosophila*. *Frontiers in Neuroscience*, *16*, 883640. https://doi.org/10.3389/fnins.2022.883640

Rybak, J., & Menzel, R. (1993). Anatomy of the mushroom bodies in the honey bee brain: The neuronal connections of the alpha-lobe. *Journal of Comparative Neurology*, *334*, 444–465. https://doi.org/10.1002/cne.903340309

Rybak, J., Kuß, A., Lamecker, H., Zachow, S., Hege, H. C., Lienhard, M., Singer, J., Neubert, K., & Menzel, R. (2010). The digital bee brain: Integrating and managing neurons in a common 3D reference system. *Frontiers in Systems Neuroscience*, *4*, 30. https://doi.org/10.3389/fnsys.2010.00030

Schachtner, J., Schmidt, M., & Homberg, U. (2005). Organization and evolutionary trends of primary olfactory brain centers in Tetraconata (Crustacea+Hexapoda). *Arthropod Structure & Development*, *34*, 257–299. https://doi.org/10.1016/j.asd.2005.04.003

Staudacher, E. (1998). Distribution and morphology of descending brain neurons in the cricket *Gryllus bimaculatus*. *Cell and Tissue Research*, *294*, 187–202. https://doi.org/10.1007/s004410051169

Staudacher, E. M., Cigan, M. L., Wenz, F., Pollun, A., Beck, S., Beck, M., Reh, F., Haas, J., & Homberg, U. (2023). Organization of descending neurons in the brain of the desert locust. *Journal of Comparative Neurology*, *531*, 1350–1380. https://doi.org/10.1002/cne.25513

Staudacher, E. M., Gebhardt, M., & Dürr, V. (2005). Antennal movements and mechanoreception: Neurobiology of active tactile sensors. *Advances in Insect Physiology*, *32*, 49–205. https://doi.org/10.1016/S0065-2806(05)32002-9

Staudacher, E., & Schildberger, K. (2000). A newly described neuropile in the deutocerebrum of the cricket: Antennal afferents and descending interneurons. *Zoology*, *102*, 212–226.

Stengl, M., & Homberg, U. (1994). Pigment-dispersing hormone-immunoreactive neurons in the cockroach *Leucophaea maderae* share properties with circadian pacemaker neurons. *Journal of Comparative Physiology A: Neuroethology, Sensory, Neural, and Behavioral Physiology*, *175*, 203–213. https://doi.org/10.1007/BF00215116

Sternberger, L. A. (1979). *Immunocytochemistry*. John Wiley and Sons.

Stone, T., Webb, B., Adden, A., Weddig, N. B., Honkanen, A., Templin, R., Wcislo, W., Scimeca, L., Warrant, E., & Heinze, S. (2017). An anatomically constrained model for path integration in the bee brain. *Current Biology*, *27*, 3069–3085. https://doi.org/10.1016/j.cub.2017.08.052

Strausfeld, N. J. (1976). *Atlas of an insect brain*. Springer.

Strausfeld, N. J. (2002). Organization of the honey bee mushroom body: Representation of the calyx within the vertical and gamma lobes. *Journal of Comparative Neurology*, *450*, 4–33. https://doi.org/10.1002/cne.10285

Strausfeld, N. J. (2005). The evolution of crustacean and insect optic lobes and the origins of chiasmata. *Arthropod Structure & Development*, *34*, 235–256. https://doi.org/10.1016/j.asd.2005.04.001

Strausfeld, N. J. (2012). *Arthropod brains: Evolution, functional elegance, and historical significance*. Belknap Press.

Strausfeld, N. J., & Bassemir, U. K. (1985a). Lobula plate and ocellar interneurons converge onto a cluster of descending neurons leading to neck and leg motor neuropil in *Calliphora erythrocephala*. *Cell and Tissue Research*, *240*, 617–640. https://doi.org/10.1007/BF00216351

Strausfeld, N. J., & Bassemir, U. K. (1985b). The organization of giant horizontal-motion-sensitive neurons and their synaptic relationships in the lateral deutocerebrum of *Calliphora erythrocephala* and *Musca domestica*. *Cell and Tissue Research*, *242*, 531–550. https://doi.org/10.1007/BF00225419

Strausfeld, N. J., & Li, Y. (1999). Organization of olfactory and multimodal afferent neurons supplying the calyx and pedunculus of the cockroach

mushroom bodies. *Journal of Comparative Neurology*, *409*, 603–625. https://doi.org/10.1002/(SICI)1096-9861(19990712)409:4

Strausfeld, N. J., Sinakevitch, I., Brown, S. M., & Farris, S. M. (2009). Ground plan of the insect mushroom body: Functional and evolutionary implications. *Journal of Comparative Neurology*, *513*, 265–291. https://doi.org/10.1002/cne.21948

Sun, L., Pan, X., Li, H., Zhang, X., Zhao, X., Zhang, L., & Zhang, L. (2022). Odor-induced vomiting is combinatorially triggered by palp olfactory receptor neurons that project to the lobus glomerulatus in locust brain. *Frontiers in Physiology*, *13*, 855522. https://doi.org/10.3389/fphys.2022.855522

Suver, M. P., Huda, A., Iwasaki, N., Safarik, S., & Dickinson, M. H. (2016). An array of descending visual interneurons encoding self-motion in *Drosophila*. *Journal of Neuroscience*, *36*, 11768–11780. https://doi.org/10.1523/JNEUROSCI.2277-16.2016

Tanaka, N. K., Tanimoto, H., & Ito, K. (2008). Neuronal assemblies of the *Drosophila* mushroom body. *Journal of Comparative Neurology*, *508*, 711–755. https://doi.org/10.1002/cne.21692

Timm, J., Scherner, M., Matschke, J., Kern, M., & Homberg, U. (2021). Tyrosine hydroxylase immunostaining in the central complex of dicondylian insects. *Journal of Comparative Neurology*, *529*, 3131–3154. https://doi.org/10.1002/cne.25151

Träger, U., Wagner, R., Bausenwein, B., & Homberg, U. (2008). A novel type of microglomerular synaptic complex in the polarization vision pathway of the locust brain. *Journal of Comparative Neurology*, *506*, 288–300. https://doi.org/10.1002/cne.21512

Vitzthum, H., Homberg, U., & Agricola, H. (1996). Distribution of Dip-allatostatin I-like immunoreactivity in the brain of the locust *Schistocerca gregaria* with detailed analysis of immunostaining in the central complex. *Journal of Comparative Neurology*, *369*, 419–437. https://doi.org/10.1002/(SICI)1096-9861(19960603)369:3

von Hadeln, J., Althaus, V., Häger, L., & Homberg, U. (2018). Anatomical organization of the cerebrum of the desert locust *Schistocerca gregaria*. *Cell and Tissue Research*, *374*, 39–62. https://doi.org/10.1007/s00441-018-2844-8

von Hadeln, J., Hensgen, R., Bockhorst, T., Rosner, R., Heidasch, R., Pegel, U., Quintero Pérez, M., & Homberg, U. (2020). Neuroarchitecture of the central complex of the desert locust: Tangential neurons. *Journal of Comparative Neurology*, *528*, 906–934. https://doi.org/10.1002/cne.24796

Warrant, E., & Dacke, M. (2011). Vision and visual navigation in nocturnal insects. *Annual Review of Entomology*, *56*, 239–254. https://doi.org/10.1146/annurev-ento-120709-144852

Wei, H., el Jundi, B., Homberg, U., & Stengl, M. (2010). Implementation of pigment-dispersing factor-immunoreactive neurons in a standardized atlas of the brain of the cockroach *Leucophaea maderae*. *Journal of Comparative Neurology*, *518*, 4113–4133. https://doi.org/10.1002/cne.22471

Wipfler, B., Letsch, H., Frandsen, P. B., Kapli, P., Mayer, C., Bartel, D., Buckley, T. R., Donath, A., Edgerly-Rooks, J. S., Fujita, M., Liu, S., Machida, R., Mashimo, Y., Misof, B., Niehuis, O., Peters, R. S., Petersen, M., Podsiadlowski, L., Schütte, K., … Simon, S. (2019). Evolutionary history of Polyneoptera and its implications for our understanding of early winged insects. *Proceedings of the National Academy of Science of the United States of America*, *116*, 3024–3029. https://doi.org/10.1073/pnas.1817794116

Wolff, T., Iyer, N. A., & Rubin, G. M. (2015). Neuroarchitecture and neuroanatomy of the *Drosophila* central complex: A GAL4-based dissection of protocerebral bridge neurons and circuits. *Journal of Comparative Neurology*, *523*, 997–1037. https://doi.org/10.1002/cne.23705

Wosnitza, A., Martin, J. P., Pollack, A. J., Svenson, G. J., & Ritzmann, R. E. (2022). The role of central complex neurons in prey detection and tracking in the freely moving praying mantis (*Tenodera sinensis*). *Frontiers in Neural Circuits*, *16*, 893004. https://doi.org/10.3389/fncir.2022.893004

Wu, M., Nern, A., Williamson, W. R., Morimoto, M. M., Reiser, M. B., Card, G. M., & Rubin, G. M. (2016). Visual projection neurons in the *Drosophila* lobula link feature detection to distinct behavioral programs. *eLife*, *5*, e21022. https://doi.org/10.7554/eLife.21022.002

Yamawaki, Y. (2019). Unraveling the functional organization of lobula complex in the mantis brain by identification of visual interneurons. *Journal of Comparative Neurology*, *527*, 1161–1178. https://doi.org/10.1002/cne.24603

Yamazaki, Y., Nishikawa, M., & Mizunami, M. (1998). Three classes of GABA-like immunoreactive neurons in the mushroom body of the cockroach. *Brain Research*, *788*, 80–86. https://doi.org/10.1016/S0006-8993(97)01515-1

Yu, H. H., Awasaki, T., Schroeder, M. D., Long, F., Yang, J. S., He, Y., Ding, P., Kao, J.-C., Wu, G. Y.-Y., Peng, H., Myers, G., & Lee, T. (2013). Clonal development and organization of the adult *Drosophila* central brain. *Current Biology*, *23*, 633–643. https://doi.org/10.1016/j.cub.2013.02.057

SUPPORTING INFORMATION

Additional supporting information can be found online in the Supporting Information section at the end of this article.

How to cite this article: Althaus, V., Exner, G., von Hadeln, J., Homberg, U., & Rosner, R. (2024). Anatomical organization of the cerebrum of the praying mantis *Hierodula membranacea*. *Journal of Comparative Neurology*, *532*, e25607. https://doi.org/10.1002/cne.25607